In mouse and gut-on-a-chip models, pre-colonoscopy bowel preparation promotes pathogen colonization of the gut and translocation to other organs

Charlotte A. Clayton[1], Giselle McCallum[1], Brian D. Deng[1], Apsara Srinivas[1], Claire Sie[1], Katharine M. Ng[1], Jerry Y. He[1], Dominique Tertigas[2], Imogen Porter[3], Deanna M. Pepin[1], Touran Fardeen[4], Sidhartha R. Sinha[4], Michael G. Surette[2,5], Bruce A. Vallance[6], Carolina Tropini[1,7,8]*

[1]Department of Microbiology & Immunology, University of British Columbia, Vancouver, British Columbia, Canada
[2]Biochemistry and Biomedical Sciences, McMaster University, Hamilton, Ontario, Canada
[3]Genome Science and Technology, University of British Columbia, Vancouver, British Columbia, Canada
[4]Department of Medicine, Division of Gastroenterology and Hepatology, Stanford University School of Medicine, Stanford, USA
[5]Department of Medicine, McMaster University, Hamilton, Ontario, Canada
[6]Department of Pediatrics, Division of Gastroenterology, Child and Family Research Institute, Vancouver, British Columbia, Canada.
[7]School of Biomedical Engineering, University of British Columbia, Vancouver, British Columbia, Canada
[8]Humans and the Microbiome Program, Canadian Institute for Advanced Research (CIFAR), Toronto, Ontario, Canada

*Corresponding Author: Carolina Tropini
Email: carolina.tropini@ubc.ca

Summary

In the United States, an estimated 14 million colonoscopies are performed yearly, each requiring patients to undergo bowel preparation, a laxative cleansing of the intestine's luminal contents. Despite the widespread use of bowel preparation, its effects on the gut and susceptibility to pathogens remains poorly understood, particularly for patients with compromised gut health. Using mouse and gut-on-a-chip models, we found that bowel preparation with the laxative polyethylene glycol rapidly alters the gut environment in multiple ways, making it more susceptible to colonization by both *Salmonella*, including a non-motile mutant normally unable to invade the gut, and gut pathobionts from an ulcerative colitis microbiota. In addition, bowel preparation promotes the translocation of these bacteria from the mouse gut to extraintestinal organs, such as nearby lymph nodes, the liver, and spleen. These findings suggest that bowel preparation may have clinical implications that are not currently appreciated.

Introduction

In the United States, an estimated 14 million colonoscopies are performed yearly[1], each requiring patients to undergo bowel preparation (prep), a laxative cleansing of the intestine's luminal contents. Bowel prep has been shown to cause significant short-term disruptions to the gut microbiota within the first several days post-procedure[2,3]. Despite the widespread use of bowel

prep, its effects on the gut environment and potential to facilitate colonization by gut pathogens remain poorly understood. Recent studies have shown that colonoscopies have significantly higher rates of infection compared to other screening procedures with some centers reporting rates of 7-day post-endoscopic infections as high as 132 per 1000 procedures[4], and a 9.38-fold increased risk of infection compared to controls that did not undergo these procedures[5].

Understanding the effects of bowel prep is especially important in vulnerable populations, including patients with inflammatory bowel disease (IBD), comprising both Crohn's disease and ulcerative colitis. In healthy individuals, microbiota composition usually returns to normal within days of bowel prep[2,3]. However, patients with IBD often harbor microbial species that can act as pathogens under certain conditions. These bacteria, known as pathobionts, are thought to worsen inflammation in IBD[6,7]. It is possible that bowel prep could create a gut environment that facilitates growth of these pathobionts; numerous cases of IBD exacerbations have been reported after patients undergo colonoscopy[8]. Previous studies have shown bowel prep may differentially affect the gut microbiota in patients with or without IBD, leading to longer-term changes in microbiota composition several weeks after the procedure[8,9], as well as adverse effects such as toxic megacolon and increased emergency room visits that have not been mechanistically linked to the procedure itself[10–15]. Understanding how bowel prep affects pathobiont growth in this population is critical, as patients with IBD undergo more frequent colonoscopies than the general population to monitor disease progression[16].

In previous work in mice, we showed that long-term (multi-day), low-concentration exposure to the laxative polyethylene glycol (PEG), used as an over the counter laxative and in human bowel prep, compromises the integrity of the intestinal mucus layer[17], an essential structure for preventing bacterial invasion of the mucosa. Moreover, PEG alters the gut microbiota and selects for bacterial species that can thrive in high osmolality environments[17,18]. In previous work, we have shown such high osmolality conditions prevent the growth of commensal bacteria[17]. In addition, studies of laxative treatment show increased susceptibility to pathogens in mice and humans[19–21]. However, these studies of pathogen susceptibility used laxatives in lower doses and longer-term regimes than are used for bowel preparation in humans. Despite the widespread use of bowel preparation, its effects on the gut microbiota, susceptibility to pathogens, and implications for patients IBD remain poorly understood. Specifically, the interactions between bowel prep-induced changes in the gut environment—such as microbiota disruption, mucus depletion, and osmolality changes—and the potential for increased pathogen susceptibility have not been elucidated. This study seeks to answer the following critical questions: (1) How does bowel preparation alter the gut microbiota and the intestinal environment, and what are the mechanisms underlying these changes? (2) Does bowel preparation increase host susceptibility to pathogenic colonization, particularly in the context of pathobionts associated with IBD? We hypothesize that bowel preparation creates an environment in the gut that facilitates the growth and colonization of osmotically resistant pathogens and pathobionts, potentially increasing systemic translocation and infection risk.

To answer these questions, in this study we established mouse and gut-on-a-chip models of bowel prep to investigate the effects of acute, high-dose laxative treatment with a time and spatial resolution not achievable in human studies. Specifically, we examined the impacts of bowel prep on the gut microbiota, the local intestinal environment, and host resistance against colonization by

Salmonella enterica serovar Typhimurium (*Salmonella* Typhimurium). To robustly colonize the intestines of mice and cause gastroenteritis, this pathogen requires disruption of the microbiota, such as via antibiotic treatment[22,23]. We found that bowel prep with PEG rapidly altered the gut environment in multiple ways, making it more susceptible to colonization by both *Salmonella* Typhimurium, including a non-motile mutant normally unable to invade the gut, and pathobionts collected from patients with ulcerative colitis. In addition, gut preparation promotes the translocation of these bacteria from the gut to extraintestinal organs, such as nearby lymph nodes, the liver, and spleen. These findings suggest that bowel prep may have clinical implications that are not currently fully appreciated.

Results

Bowel preparation disrupts intestinal osmolality, the mucus layer, and short-chain fatty acid levels in the mouse gut

We hypothesized that bowel prep would lead to a significant disruption of the gut environment and reduction of levels of bacteria and bacterially produced compounds given the severe diarrhea caused by this procedure. To mimic the human bowel prep process, we investigated the impact of short-term, high-concentration PEG exposure on the gut's mucosal lining. We fixed, stained, and imaged the cecum and colon mucosal layers of C57BL/6J mice orally gavaged with PEG (bowel prep) or water (vehicle) four times, at 20-minute intervals (**Fig. 1A**). Bowel prep-treated mice had an average cecal osmolality that was 1.8-fold higher than vehicle-treated controls (724 vs. 438 mOsm/Kg, $p < 0.001$) (**Fig. 1B**) and a higher cecal mass, indicative of osmotic diarrhea, and increased water excretion during bowel prep (**Fig. S1A**). At 6 hours after treatment, the distal colon of vehicle-treated mice displayed the expected thick, continuous mucus layer, whereas that of bowel prep-treated mice revealed a largely depleted mucus layer (**Fig. 1C**), despite having normal weight (**Fig. S1A**). In addition, the percentage of epithelium covered with mucus was 64% lower in bowel prep - vs vehicle-treated mice (79.1% vs 28.7%, $p = 0.02$), and the average thickness of the mucus layer was 75% lower (22.8 vs 6.0 µm, $p = 0.02$; **Fig. 1C, S1B**). Upstream in the cecum, the mucus layer in vehicle-treated mice was more hydrated and patchier than in the distal colon, as expected[24,25]. Here, the percentage of the epithelium covered with mucus was 85% lower in bowel prep- vs vehicle-treated mice (48.8% vs 9.2%, $p = 0.03$), and mucus layer thickness was 81% lower (8.3 vs 1.2 µm, $p = 0.03$; **Fig. 1D, S1B**). These findings indicate that even short-term, high-concentration PEG exposure can severely disrupt the protective mucus barrier in the gut.

We wondered whether the disruption of the mucus layer might lead to abnormalities in the tissue. We therefore assessed pathology in hematoxylin and eosin (H&E)-stained sections of the cecum and distal colon, including in the lumen, epithelium, mucosa, and submucosa. No immune cell infiltration was observed in samples from bowel prep- or vehicle-treated mice. In the cecum, mucosa thickness was significantly lower in bowel prep- vs vehicle-treated mice (50.2 vs 100.1 µm, $p = 0.002$; **Fig. 1E, S1C**). This reduction in mucosa thickness was not observed in the distal colon (120.6 vs 123.0 µm, $p = 0.7922$; **Fig. 1E**). This suggests that bowel preparation–induced excretion of water, which reduces mucosa thickness, is not uniform throughout the gut.

Next, we measured how bowel prep treatment affects gut microbiota in mice. We hypothesized that the bacterial loads would be significantly decreased, and the membership changed. To test this hypothesis, we cultured bacteria from the gut both anaerobically and aerobically to measure

136 bacterial loads, as diarrhea is thought to increase oxygen levels in the gut[26]. In the distal colon and
137 small intestine, culturable anaerobic bacterial loads were lower in bowel prep- vs vehicle-treated
138 mice (3.6×10^9 vs 1.6×10^{10} CFU/mL, $p = 0.01$ and 8.4×10^8 vs 1.0×10^{10} CFU/mL, $p = 0.009$,
139 respectively), but in the cecum, bacterial loads did not differ between the two treatment groups
140 (**Fig. 1F, Fig. S1D**). By contrast, culturable aerobic bacterial loads in the distal colon and small
141 intestine, while a much smaller percentage of the total counts (0.07% and 0.03% respectively in
142 the vehicle), were similar between the two treatment groups; in the cecum, they were 17-fold
143 higher in bowel prep- vs vehicle-treated mice (1.6×10^8 vs 9.6×10^6 CFU/mL, $p = 0.005$; **Fig. 1F,**
144 **Fig. S1D**). These findings indicate an overall reduction in microbial load due to bowel prep, and
145 the expansion of aerobic bacteria, consistent with oxygenation of the gut environment. The
146 composition of the cecal microbiota 6 hours post-treatment, as measured by 16S rRNA sequencing,
147 was largely similar in bowel prep- vs vehicle-treated mice (**Fig. 1G**). Combined with the bacteria
148 load data, this observation suggests that 16S rRNA sequencing is measuring a portion of the
149 microbiota that is either not culturable or no longer alive post-bowel preparation.
150
151 Given the changes in microbial load, we expected to find lower levels of microbial metabolites in
152 the gut. To test this hypothesis, we measured individual short-chain fatty acid (SCFA) levels in
153 the cecum's contents, as major site of microbial activity in the mouse intestine. SCFA levels were
154 significantly lower in bowel prep- vs vehicle-treated mice (3.9-, 17.4- and 5-fold lower, $p = 0.03$
155 for acetic, butyric and propionic acid, respectively; **Fig. 1H, S1E**). We also measured the pH of
156 the cecal contents as it is affected by SCFA levels and can impact bacterial growth and
157 composition[18]; however, cecal pH did not differ between the treatment groups (**Fig. S1F**). These
158 findings support the hypothesis that bowel preparation leads to a significant disruption of the gut
159 environment and impairs microbial metabolism. Given the importance of SCFAs and mucus to
160 enteric pathogen infection[27,28], these results suggest that the post bowel-prep gut environment may
161 provide diminished colonization resistance against invading bacteria.
162

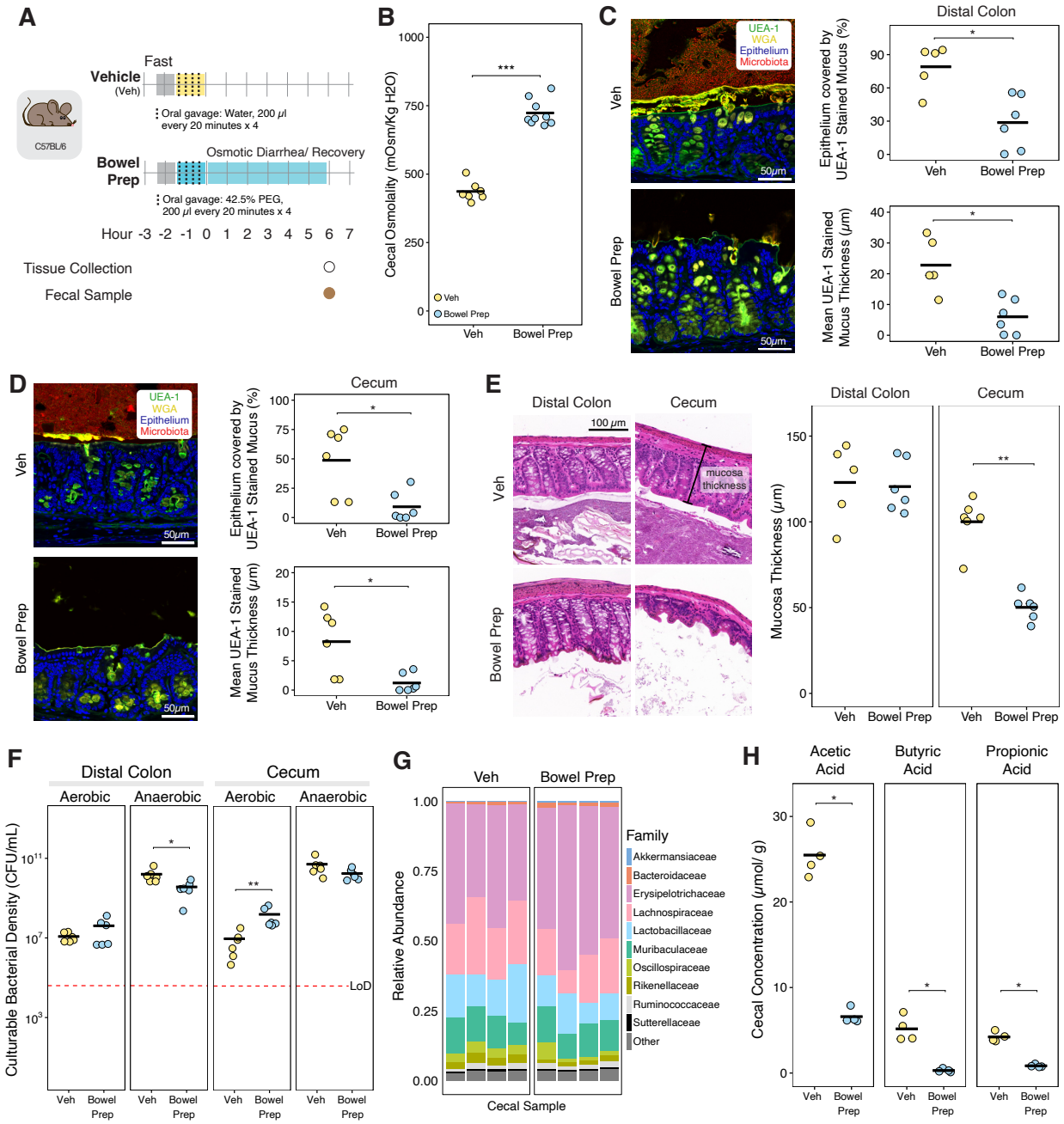

Figure 1. Bowel preparation with a laxative (polyethylene glycol, PEG) disrupts intestinal osmolality, the mucus layer, and short-chain fatty acid (SCFA) levels 6-hours post procedure in the mouse gut. (A) Schematic representation of our mouse model for bowel preparation. Mice were orally gavaged four times with 42.5% PEG in water (bowel prep) or water (vehicle, Veh), at 20-minute intervals. (B) Cecal osmolality was significantly higher in bowel prep- vs vehicle-treated mice (Veh *n*=7, Bowel Prep *n*=9). (C) *Left*: 6 hours post-treatment, a representative confocal micrograph of the distal colon shows the mucus layer (indicated by staining with UEA-1 [*green*] and WGA [*yellow*]) is considerably thinner in bowel prep- vs vehicle-treated mice. Epithelial cell nuclei (*blue*) and bacteria (*red*) were stained with DAPI *Right*: The percentage of epithelium covered by mucus (*top*) and mucus layer thickness (*bottom*), quantified using UEA-1 fluorescence, were significantly lower in bowel prep- vs vehicle-treated mice (Veh *n*=5, Bowel Prep

n=6). (D) *Left*: 6 hours post-treatment, a representative confocal micrograph of the cecum, stained and analyzed as in (C), shows the mucus layer is considerably thinner in bowel prep- vs vehicle-treated mice. *Right*: The percentage of epithelium covered by mucus (*top*) and mucus layer thickness (*bottom*), quantified using UEA-1 fluorescence (*green*), were significantly lower in bowel prep- vs vehicle-treated mice (Veh *n*=6, Bowel Prep *n*=6). (E) *Left*: 6 hours post-treatment, representative images of hematoxylin and eosin (H&E)-stained sections of the distal colon and cecum show no evidence of immune cell infiltration. *Right*: For both colon and cecum, mucosa thickness in the stained sections is significantly lower in bowel prep- vs vehicle-treated mice (Veh *n*=6, Bowel Prep *n*=6). (F) 6 hours post-treatment, in the distal colon, loads of culturable anaerobic bacteria were significantly higher in bowel prep- vs vehicle-treated mice, whereas in the cecum, loads of culturable aerobic bacteria were significantly higher (Veh *n*=6, Bowel Prep *n*=6). (G) 6 hours post-treatment, 16S rRNA sequencing of the contents of the cecum shows that the relative abundance of various bacterial families is similar between bowel prep- and vehicle-treated mice. (H) 6 hours post-treatment, in the contents of the cecum, the abundance of three SCFAs, measured using gas chromatography-mass spectrometry, was significantly lower in bowel prep- vs vehicle-treated mice (Veh *n*=4, Bowel Prep *n*=4). **Statistics**: For all comparisons, statistical significance was assessed using the Wilcoxon ranked-sum test. $p > 0.05$; ns (not significant, not shown), $p < 0.05$; *, $p < 0.01$; **, $p < 0.001$; ***, $p < 0.0001$; ****. **Abbreviation**: LoD, limit of detection.

Bowel preparation promotes *Salmonella* Typhimurium colonization, translocation, and pathology in mice

Having observed that bowel prep treatment reduces the thickness and coverage of the gut mucus layer, SCFA levels and increases intestinal osmolality (**Fig. 1B**), we hypothesized that enteric pathogens would be able to bypass colonization resistance more easily in bowel prep- vs vehicle-treated mice. Specifically, given that commensal microbiota members are highly sensitive to osmolality[17,18], we reasoned that an osmotically-resilient pathogen may be advantaged during bowel prep. To test this hypothesis, we measured growth rates of *Salmonella* Typhimurium, an enteric bacterial pathogen known for its ability to withstand osmotic stress in high-salt environments[29], in growth media adjusted with PEG to various osmolality levels. At an osmolality comparable to that observed in the post-bowel preparation gut of mice (~800 mOsm/Kg), *Salmonella* Typhimurium growth in culture was indistinguishable from growth under normal osmotic conditions (~450 mOsm/Kg; **Fig. 2A**). Next, we challenged bowel prep- and vehicle-treated mice with a standard infectious dose of 10^6 CFU *Salmonella* Typhimurium via oral gavage (**Fig. 2B**). Whereas vehicle-treated mice showed no detectable levels of *Salmonella* Typhimurium in their feces post-treatment, bowel prep-treated mice showed high levels of colonization (**Fig. 2C**). One day after inoculation, fecal *Salmonella* Typhimurium levels in bowel prep-treated mice reached 2 x 10^9 CFU/mL; these levels persisted at least 3 days post-inoculation, indicating expansion of the pathogen in the intestinal tract (**Fig. 2C**). This finding was not sex-dependent (**Fig. S2A**). These results support our hypothesis that bowel preparation–induced disruption of the gut environment facilitates colonization and growth by osmotically resistant enteric pathogens.

Next, we investigated whether *Salmonella* Typhimurium could translocate from the gut to extraintestinal organs. Given the removal of the mucus layer and disruption of the microbiota, we hypothesized that *Salmonella* Typhimurium would be able to reach extra-intestinal organs. Supporting this hypothesis, three days post-inoculation, we identified significant colonization in the mesenteric lymph nodes (4.2 x 10^6 CFU/g), spleen (4.2 x 10^4 CFU/g), and liver (3.2 x 10^4 CFU/g) of bowel prep-treated mice (**Fig. 2D**). No colonization of these organs was observed in

vehicle-treated mice, indicating that in normal conditions *Salmonella* Typhimurium translocation is at best a very rare event.

We also used H&E staining to visualize the host tissue to *Salmonella* Typhimurium in the mouse cecum and distal colon and to assess its integrity 3 days post infection. Given *Salmonella* Typhimurium was able to translocate to extra-intestinal organs, we hypothesized that there would be significant pathology in the intestinal tissues. Supporting this hypothesis, in the cecum, combined histopathological scores for the lumen, epithelium, mucosa, and submucosa were significantly higher in bowel prep- vs vehicle-treated mice (**Fig. 2E,F**). No significant difference in histopathological scores between the treatment groups was found for the distal colon, suggesting that during bowel prep the cecum is the primary site of infection.

The standard model for *Salmonella* Typhimurium infection involves pre-treating mice with antibiotics to deplete colonization resistance by native gut microbiota[30] and we wanted to compare the efficacy of pathogen colonization in these two models. Therefore, we compared the *Salmonella* Typhimurium load in mice treated with bowel prep or streptomycin prior to inoculation (**Fig. S2B-D**). Three days after infection, the maximum fecal burden (as a measure of highest infection level) of *Salmonella* Typhimurium was 11-fold higher in streptomycin- vs bowel prep-treated mice (**Fig. S2B**). However, *Salmonella* Typhimurium levels in the extraintestinal organs were similar between the streptomycin- and bowel prep-treated mice (**Fig. 2D, S2D**) and significant pathology was observed (**Fig. S2E,F**). The similar levels of extra-intestinal translocation despite differing intestinal levels suggest that *Salmonella* Typhimurium expansion in the organs may dictate the ultimate colonization levels there rather than the abundance in the intestine. Altogether, these findings indicate that bowel preparation alone, without antibiotics, can facilitate expansion of *Salmonella* Typhimurium in the gut and its translocation to extraintestinal sites.

Finally, we investigated the minimum dose required for *Salmonella* Typhimurium to colonize the gut of mice subjected to bowel preparation. We hypothesized that a dose lower than 10^6 CFU would still enable robust gut colonization and translocation by *Salmonella* Typhimurium, as bowel prep treatment would create a gut environment vulnerable to even low levels of pathogen. Supporting this hypothesis, among bowel prep-treated mice, inoculation with as few as 1,000 CFU led to most mice becoming colonized (**Fig. 2G**). In addition, in bowel prep-treated mice, *Salmonella* Typhimurium translocation levels 3 days after inoculation largely increased with the size of the dose administered (**Fig. 2H**). These findings indicate that a much lower minimum dose of *Salmonella* Typhimurium is required to colonize the gut after bowel preparation, and the higher the dose, the higher the level of translocation to extraintestinal organs.

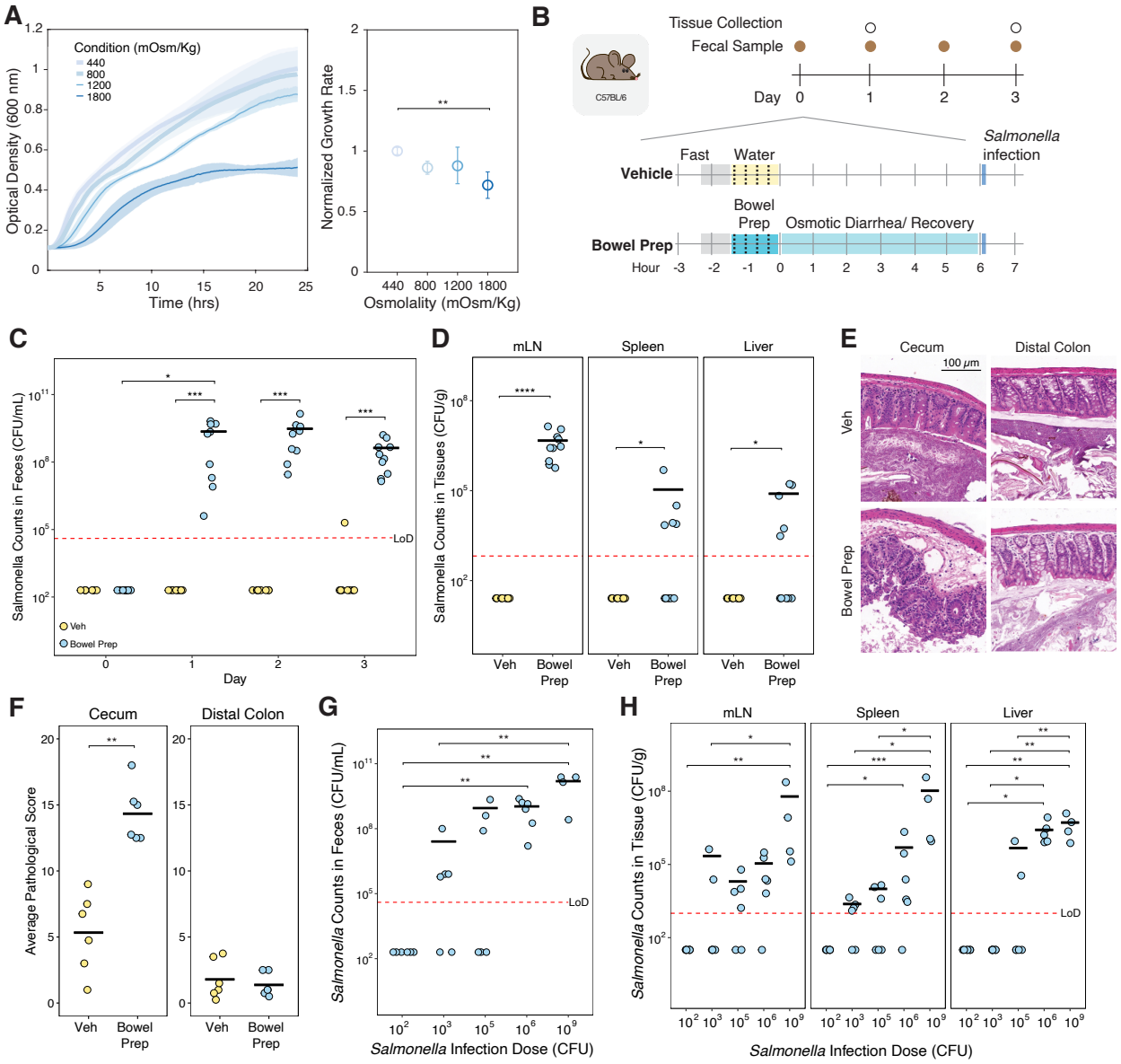

Figure 2. Bowel preparation with a laxative (polyethylene glycol, PEG) promotes *Salmonella enterica* serovar Typhimurium colonization, translocation, and gut pathology in mice.
(A) In culture, *Salmonella* Typhimurium growth rates are similar under normal osmotic conditions (~450 mOsm/Kg) and osmotic conditions comparable to those in the post-bowel preparation gut of mice (~800 mOsm/Kg) (each osmolality *n*=4). Growth curves were estimated by measuring optical density (OD600) over time in aerobic media with various osmotic levels (obtained with varying PEG concentrations). Growth rates were compared using a one-way ANOVA with Tukey's post-hoc test for multiple comparison (each osmolality *n*=4). (B) Schematic of our bowel preparation-pathogen mouse model. Mice were infected with *Salmonella* Typhimurium 6 hours after bowel preparation with PEG. (C) Starting 1 day after inoculation, *Salmonella* Typhimurium counts were significantly higher in the feces of bowel prep- vs vehicle-treated mice (Veh *n*=8, Bowel Prep *n*=10). Differences between timepoints were analyzed with a Wilcoxon ranked-sum test, and differences between bowel prepped-samples at different timepoints were analyzed with a Friedman test followed by Nemenyi post-hoc test. (D) Three days after inoculation, *Salmonella* Typhimurium translocation levels from the gut to the mesenteric lymph nodes

(mLN), liver, and spleen were significantly higher in bowel prep- vs vehicle-treated mice (Veh *n*=8, Bowel Prep *n*=10). Counts in the extraintestinal organs were measured via plating. Differences between groups were analyzed with a Wilcoxon ranked-sum test. (E) Representative images of H&E-stained sections of the distal colon and cecum in bowel prep - vs vehicle-treated mice inoculated with 10^6 CFU of *Salmonella* Typhimurium show that 3 days post-inoculation the cecum morphology is changed in bowel prep- vs vehicle-treated mice unlike the colon. (F) Histopathological scores of the distal colon and cecum sections from (E) were significantly higher in bowel prep-vs vehicle-treated mice (Veh *n*=6, Bowel Prep *n*=6). Differences between groups were analyzed with a Wilcoxon ranked-sum test. (G) By day 3 post-inoculation, detectable levels of translocated *Salmonella* Typhimurium were observed in the feces of mice treated with bowel prep and inoculated with doses exceeding 1,000 CFU (100-10^6 CFU *n*=6, 10^9 CFU *n*=4). Differences between groups were analyzed with Kruskal-Wallis followed by Dunn's post-hoc test. (H) At day 3 post-inoculation, *Salmonella* Typhimurium translocation levels from the gut to the mesenteric lymph nodes (mLN), spleen, and liver in bowel prep-treated mice show a rough dose-response relationship with pathogen inoculation dose (100-10^6 CFU *n*=6, 10^9 CFU *n*=4). Differences between timepoints were analyzed with Kruskal-Wallis followed by Dunn's post-hoc test. $p > 0.05$; ns (not significant, not shown), $p < 0.05$; *, $p < 0.01$; **, $p < 0.001$; ***, $p < 0.0001$; ****. **Abbreviation**: LoD, limit of detection.

The longer the period between bowel preparation and inoculation with *Salmonella* Typhimurium, the greater the resistance to pathogen colonization in mice

In light of our finding that bowel prep treatment increased the susceptibility of mice to colonization by *Salmonella* Typhimurium, we investigated which physiological differences might be responsible. Having observed that bowel prep treatment significantly increased pathological scores in the cecum (**Fig. 2E,F**), we characterized the cecal environment in mice at different timepoints post-bowel preparation. Cecal osmolality recovered rapidly after bowel prep treatment (765 mOsm/Kg); 24 hours after bowel preparation, values were similar to those at baseline (479 vs 423 mOsm/Kg, $p = 0.02$) (**Fig. 3A**). Cecal mucus coverage and thickness also recovered to baseline values 24 hours after bowel preparation (**Fig. 3B, S3A-C**). However, cecal and fecal microbiota composition, as measured by Bray Curtis dissimilarity values, remained altered 48 hours post-bowel preparation (**Fig. 3C**). Similarly, species diversity levels remained lower than at baseline 24 and 48 hours after bowel prep treatment (**Fig. 3D**). Finally, SCFA concentrations, particularly for butyrate, remained depleted in bowel prep-treated mice 24 hours after treatment but recovered by 48 hours (**Fig. 3E, S3D**).

To investigate whether these changes to the gut environment impact resistance to pathogen colonization, we challenged mice with *Salmonella* Typhimurium 6, 24, and 48 hours after bowel prep treatment (**Fig. 3F**). Seventy-two hours after inoculation, fecal *Salmonella* Typhimurium levels were high in mice inoculated 6 hours after bowel prep treatment but lower in mice inoculated 48 hours after treatment (**Fig. 3G**). Similarly, 72 hours after inoculation, *Salmonella* Typhimurium levels in the mesenteric lymph nodes were high in mice inoculated 6 and 24 hours after bowel prep treatment but lower in mice inoculated 48 hours after treatment (**Fig. 3H**). The high levels of fecal *Salmonella* Typhimurium observed at timepoints when the microbiota and SCFA levels were still depleted suggests that microbiota-related factors play an important role in resistance against colonization by this pathogen.

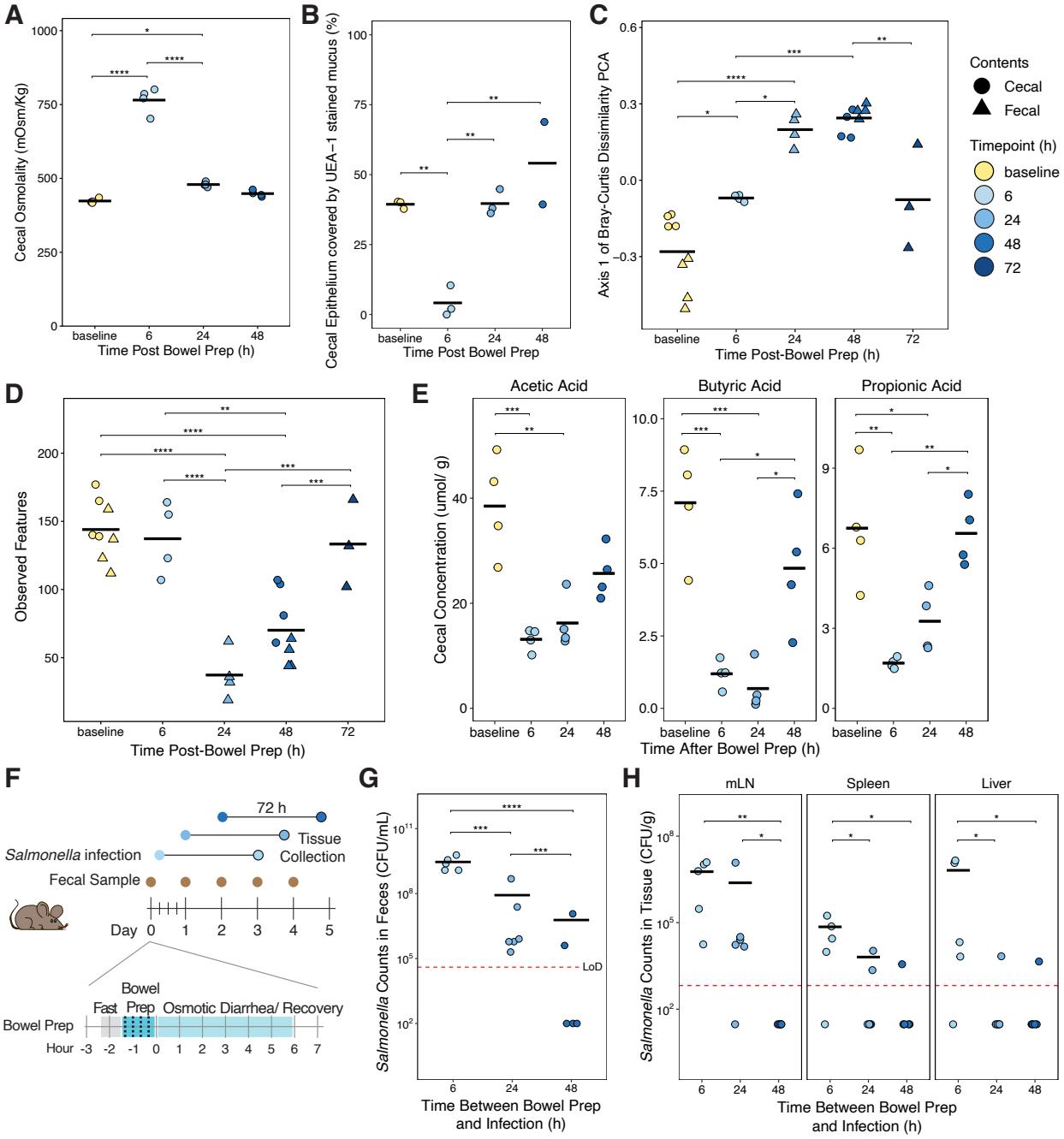

Figure 3. The longer the period between bowel preparation and inoculation with *Salmonella enterica* serovar Typhimurium, the greater the resistance to pathogen colonization in mice.
(A) Cecal osmolality increases dramatically 6 hours after bowel preparation with the detergent laxative polyethylene glycol (PEG) but largely recovers within 24 hours (each timepoint *n*=4). Differences between timepoints were analyzed using t-tests. (B) In the cecum, mucus coverage of the epithelium, as measured with UEA-1 staining, is significantly lower 6 hours after bowel prep treatment than at baseline, but coverage has recovered 24 hours after treatment (baseline-24h *n*=3, 48h *n*=2). Differences between timepoints were analyzed using a one-way ANOVA with Tukey's post-hoc test for multiple comparisons. (C) Bray Curtis dissimilarity values for the cecal and fecal microbiome, determined from 16S rRNA sequencing, increase

after bowel prep treatment by 6 hours post bowel prep but are not significantly different from baseline 72 hours post-treatment (baseline *n*=8, 6h *n*=4, 24h *n*=4, 48h *n*=8, 72h *n*=3). Differences between timepoints were analyzed using a one-way ANOVA with Tukey's post-hoc test for multiple comparisons. (D) The number of observed features (alpha diversity) in the cecal and fecal microbiome, determined from 16S rRNA sequencing, decreased after bowel prep treatment until the 24-hour timepoint, after which values began to recover (baseline *n*=8, 6h *n*=4, 24h *n*=4, 48h *n*=8, 72h *n*=3). Differences between timepoints were analyzed using a one-way ANOVA with Tukey's post-hoc test for multiple comparisons. (E) Abundance of three short-chain fatty acids in the cecum, measured by gas chromatography-mass spectrometry, was significantly lower 6 hours after bowel prep treatment than at baseline, but substantial recovery was evident by the 48-hour timepoint (each timepoint *n*=4). Differences between timepoints were analyzed with Kruskal-Wallis followed by Dunn's post-hoc test. (F) Schematic of our bowel preparation–pathogen mouse model with *Salmonella* Typhimurium inoculation at 6, 24 and 48 hours after bowel prep treatment. (G) The longer the period between bowel preparation with bowel prep and inoculation, the lower the levels of fecal *Salmonella* Typhimurium in mice (6h *n*=5, 24h *n*=6, 48h *n*=5). Culturing of organs to obtain pathogen counts was performed 72 hours post-inoculation. Differences between timepoints were analyzed with Kruskal-Wallis followed by Dunn's post-hoc test. (H) The longer the period between bowel preparation with PEG and inoculation, the lower the levels of *Salmonella* Typhimurium translocation from the gut to the mesenteric lymph nodes (mLN), liver, and spleen (6h *n*=5, 24h *n*=6, 48h *n*=5). Culturing of organs to obtain pathogen counts was performed 72 hours post-inoculation. Differences between timepoints were analyzed with Kruskal-Wallis followed by Dunn's post-hoc test. LoD, limit of Detection. $p > 0.05$; ns (not significant, not shown), $p < 0.05$; *, $p < 0.01$; **, $p < 0.001$; ***, $p < 0.0001$; ****.

Flagellar motility is not required for *Salmonella* Typhimurium to colonize the gut or translocate to lymph nodes after bowel preparation in mice

Normally, flagellar propulsion is critical for *Salmonella* Typhimurium and other bacterial pathogens to penetrate the mucus layer of the gut and infect the underlying epithelium[31,32]. However, given the defects in the cecal mucus layer that we observed 6 hours after bowel prep treatment (**Fig. 3B**), we hypothesized that a non-motile *Salmonella* Typhimurium mutant might be able to colonize mice that had undergone bowel preparation. To test this hypothesis, we challenged mice with wild-type *Salmonella* Typhimurium or a non-motile *Salmonella* Typhimurium *ΔflhD* mutant 6 hours after bowel prep or vehicle treatment. The *ΔflhD* mutant is missing the gene responsible for control of flagellar production[33] but, like wild-type *Salmonella* Typhimurium, is resilient to osmotic perturbation (**Fig. S4**). Consistent with our hypothesis, mice treated with bowel prep and inoculated with the *Salmonella* Typhimurium *ΔflhD* mutant were efficiently colonized by the pathogen, whereas mice treated with vehicle were not (**Fig. 4A**). In addition, as hypothesized, among bowel prep-treated mice, fecal levels of the *ΔflhD* mutant were comparable to those of wild-type *Salmonella* Typhimurium 1 day after inoculation (**Fig. 4A,B**). Finally, the *ΔflhD* mutant was able to translocate from the gut to the mesenteric lymph nodes in bowel prep - treated mice but not vehicle-treated mice, though its ability to translocate to the spleen and liver was limited, especially when compared to that of wild-type *Salmonella* Typhimurium (**Fig. 4C, 2D**). These observations indicate that bowel preparation–induced disruption of the gut's mucus layer allows *Salmonella* Typhimurium to colonize the gut and translocate to nearby lymph nodes without the normal requirement for motility.

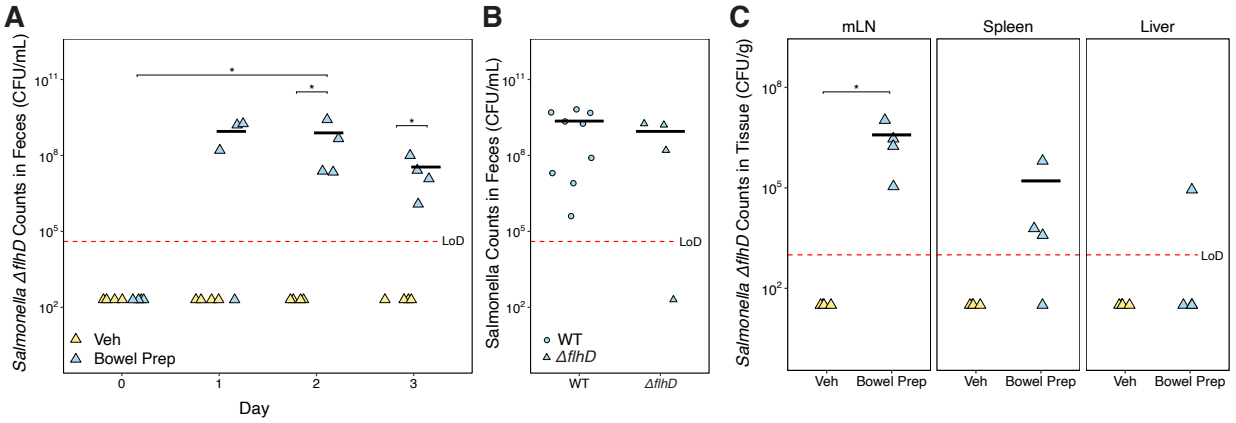

Figure 4. Flagellar motility is not required for a *Salmonella enterica* serovar Typhimurium mutant (*ΔflhD*) to colonize the gut or translocate to nearby lymph nodes in mice subjected to bowel preparation with a laxative (polyethylene glycol, PEG) 6 hours earlier.
(A) *Salmonella* Typhimurium *ΔflhD* is able to colonize the guts of bowel prep- but not vehicle-treated mice (Veh *n*=4, Bowel Prep *n*=4). Pathogen counts were measured by plating feces over a 3-day period after inoculation. Differences in timepoints were analyzed Wilcoxon ranked-sum test, and differences between bowel prepped-samples at different timepoints were analyzed with a Friedman test followed by Nemenyi post-hoc test. (B) Among bowel prep-treated mice, wild-type (WT) and *ΔflhD Salmonella* Typhimurium counts in the feces were similar 1 day after inoculation (WT *n*=9 from Fig 2C, *ΔflhD n*=4). The differences between the treatment groups was measured using the Wilcoxon ranked-sum test. (C) Among bowel prep- but not vehicle-treated mice, *Salmonella* Typhimurium *ΔflhD* was able to translocate from the gut to the mesenteric lymph nodes (mLN), but not to the spleen or liver (Veh *n*=4, Bowel Prep *n*=4). Translocation in organ tissue 72 hours after bowel preparation. Differences between treatment groups were measured using the Wilcoxon ranked-sum test. **Abbreviation**: LoD, limit of detection.

In mice, bowel preparation induces limited changes in host gene expression, including genes responsible for mucus layer production

To investigate whether a bowel preparation–induced decrease in host mucus production is responsible for depleting the gut's mucus layer and increasing vulnerability to infection, we analyzed the transcriptome of mouse cecal tissue at various timepoints after bowel prep treatment (**Fig. 5, S5**). We hypothesized that genes involved in host mucus production would be downregulated after bowel preparation. Six hours post-bowel preparation, at the height of osmotic diarrhea, gene expression was largely unchanged from baseline (**Fig. 5A**). This included expression of genes involved in mucus layer production, antimicrobial peptide production, tight junction maintenance and cellular stress responses (Table S1). The small number of genes whose expression changed 6 hours after bowel prep, none of which included genes responsible for mucus layer production, suggests that the differences we observed in the gut environment at this timepoint were driven by the treatment itself rather than by a host response. Furthermore, also seventy-two hours post-bowel preparation, expression of genes involved in mucus production remained largely unchanged from the baseline and 6-hour timepoints (**Fig. 5B**). These results suggest that the differences we observed in the gut environment at this timepoint were driven by the treatment itself rather than by a host response.

405 **In a human gut-on-a-chip, bowel preparation induces rapid changes in epithelial layer**
406 **permeability and the ability of *Salmonella* Typhimurium to translocate from the luminal side**
407 **to past the endothelial layer**
408 Next, we investigated whether alterations in the mechanical integrity of the epithelial layer,
409 specifically permeability, could be responsible for the increased vulnerability to pathogen
410 colonization observed in mice that received bowel preparation. To test this hypothesis, we
411 investigated the ability of *Salmonella* Typhimurium to invade human cell lines under normal and
412 bowel preparation–like conditions using an Emulate gut-on-a-chip S1 device, which replicates
413 intestinal movements and fluid flow in the human gut (**Fig. 5B,C**). Caco-2 and HT-29 cells, a
414 well-established model of the intestinal epithelium[34], were co-cultured on the chip with human
415 intestinal microvascular endothelial cells, allowing an epithelial barrier to form. After 7 days, we
416 exposed some chips to bowel prep-supplemented media and 5x higher basal flow conditions for
417 30 minutes, to simulate bowel preparation conditions. Then, both bowel prep-treated and control
418 chips were challenged with 10^6 CFU/mL *Salmonella* Typhimurium. After 4 hours, bowel prep-
419 treated chips showed a 5-fold increase in mean average apparent permeability relative to control
420 chips (**Fig. 5D**). After 24 hours, permeability trended higher in bowel prep-treated chips,
421 although the difference between treatment groups was smaller, likely due to damage caused by
422 *Salmonella* Typhimurium to both types of chip. In addition, mean *Salmonella* Typhimurium
423 translocation from the luminal side (top channel) to past the endothelial layer (bottom channel)
424 was 3.2-fold higher in bowel prep-treated vs control chips, though not statistically different (**Fig.**
425 **5E**). These results confirm the ability of bowel preparation to increased gut permeability and
426 susceptibility to *Salmonella* Typhimurium translocation in a simulated human gut environment.
427
428

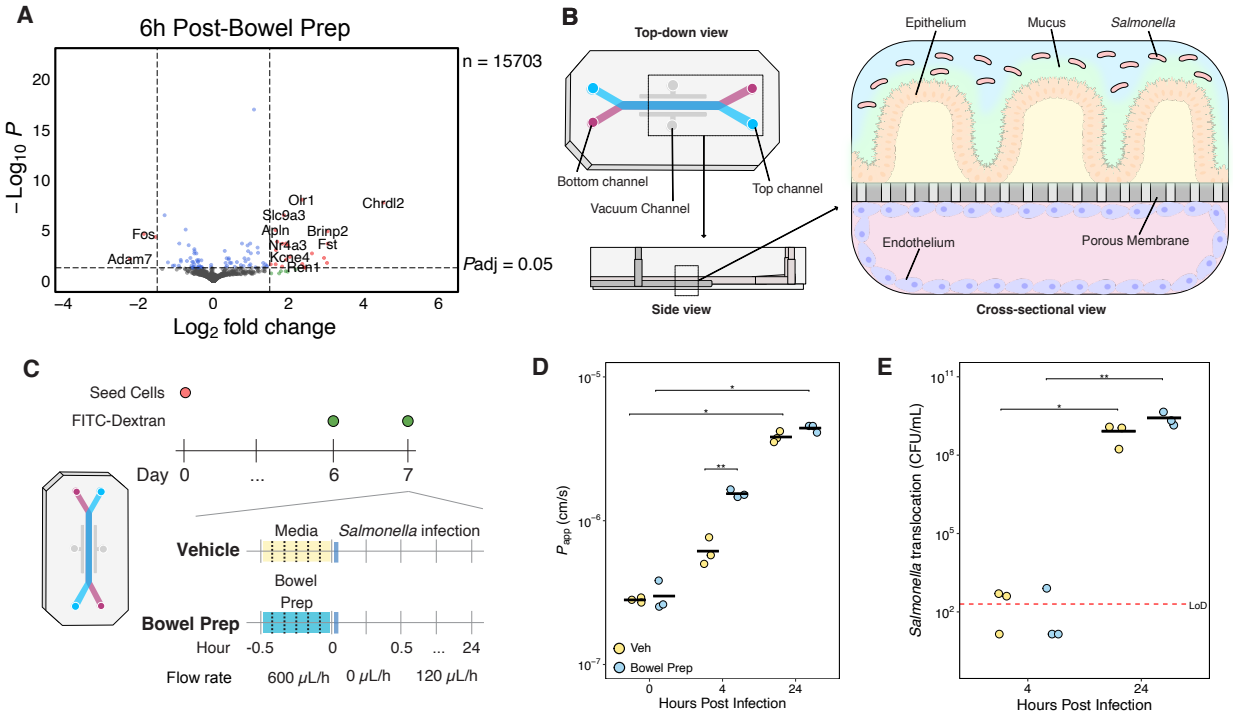

Figure 5. Bowel preparation with a detergent laxative (polyethylene glycol, PEG) minimally impacts gene expression in mice, but increases epithelial layer permeability and the ability of *Salmonella enterica* serovar Typhimurium to translocate from the luminal side to past the endothelial cell layer in a simulated human gut environment.
(A) Volcano plot of differential gene expression in mouse cecal tissue at baseline and 6 hours after PEG treatment shows few genes were differentially expressed, including genes involves in gut mucus layer production (Data Table S1). The plot shows the names of genes with adjusted p-values (Benjamin-Hochberg false discovery rate–corrected) <0.05 and Log_2 fold change >1.5. (B) Heat map of gene expression at 0, 6, and 72 hours after bowel prep-treatment of the mice from (A) shows genes involved in mucus layer production, antimicrobial peptide production, tight junction maintenance, and cellular stress responses are not significantly affected by bowel prep treatment. (C) Schematic of gut-on-a-chip experiment designed to simulate the human gut environment, with top down, side, and cross-sectional views. (D) Apparent permeability (P_{app}) of the gut epithelial layer on the gut-on-a-chip, as measured by FITC-dextran permeability assay, was 2.5-fold higher in bowel prep- vs vehicle-treated chips 4 hours after exposure to *Salmonella* Typhimurium (Veh *n*=3, Bowel Prep *n*=3). Differences in timepoints were analyzed with a t-test, and differences between treatment groups at each timepoint were analyzed with a Friedman test followed by Nemenyi post-hoc test. Each dot corresponds to one chip, with mean P_{app} for a treatment group/time period shown as black bars. (E) The amount of *Salmonella* Typhimurium translocation from the luminal side (top channel) to past the endothelial layer (bottom channel) in the experiment from (D) was 3.2-fold higher in bowel prep- vs vehicle -treated chips 24 hours post-pathogen exposure (Veh *n*=3, Bowel Prep *n*=3). Differences between treatment groups and timepoints were both analyzed using t-tests. Each dot corresponds to one chip, with mean CFU/mL for a treatment group/time period shown as black bars. **Abbreviation**: LoD, limit of detection.

454 **Pathobionts from patients with inflammatory bowel disease are resilient to osmotic**
455 **perturbation *in vitro* and can translocate and persist in the mesenteric lymph nodes of**
456 **humanized mice post-bowel preparation**
457 Having demonstrated that exogenously introduced *Salmonella* Typhimurium can escape the gut
458 and reach extraintestinal organs in a mouse model of bowel preparation, we hypothesized that
459 bacteria already present in the microbiota could also exploit the disrupted environment to
460 translocate to extraintestinal organs. To test our hypothesis, we investigated the ability of 130
461 potential pathobionts isolated from patients with ulcerative colitis (family Enterobacteriaceae,
462 genera: *Proteus, Morganella, Kluyvera, Klebsiella, Escherichia, Enterobacter* and *Citrobacter*) to
463 grow in culture under various conditions simulating bowel preparation. First, we varied osmolarity
464 levels. The pathobionts showed strong growth at osmotic levels experienced in the mouse gut post-
465 bowel preparation (~765 mOsm/Kg) in both anaerobic and aerobic conditions (**Fig. 6A, Fig. S6A**).
466 In fact, most strains were able to grow above 1100 mOsm/Kg. These results indicate that
467 pathobionts can thrive under the osmotic conditions created by bowel preparation.
468
469 Next, we asked whether the pathobionts' relatively high osmotic resistance could lead to a shift in
470 community composition under conditions of continued elevated osmotic stress. We cultured a fecal
471 sample obtained from an individual with ulcerative colitis under osmotic stress levels simulating
472 normal (400 mOsm/Kg) and bowel prep-treated (800 mOsm/Kg) conditions. 16S rRNA sequence
473 data showed a shift in community composition under the high osmolality condition (**Fig. 6B**),
474 including increased abundance of the family Enterobacteriaceae. Specifically, the abundance of
475 the genera *Morganella* and *Escherichia-Shigella* increased (**Fig. 6C**), indicating that even in a
476 complex community, these potential pathobionts had a competitive advantage.
477
478 We then investigated the ability of potential pathobionts to translocate from the gut to extra-
479 intestinal organs and persist there, in a mouse model of bowel preparation. To do so, we
480 inoculated germ-free mice with a fecal sample from either a person with ulcerative colitis or a
481 healthy human control. We then bred the mice and treated the offspring with PEG (**Fig. S6B**). As
482 a further control, we performed bowel prep on mice with a conventional mouse microbiota. In
483 each animal, we detected no significant translocation to extraintestinal organs 2 weeks post-
484 bowel preparation compared to baseline (**Fig. S6C**).
485
486 Because we were interested in the impact of bowel preparation on patients with IBD, some of
487 whom have a genetic predisposition to increased permeability of the gut epithelium[35], we
488 repeated this experiment in humanized germ-free Swiss Webster mice with the fecal sample
489 from the patient with ulcerative colitis. This outbred mouse strain exhibits greater variability in
490 susceptibility to infectious agents than inbred strains such as C57BL/6J[36]. Translocation to
491 extraintestinal organs was increased at 24 hours post-bowel preparation, but increased number of
492 bacteria remained in the lymph nodes even 2 weeks later (**Fig. 6D**). Sequence data identified the
493 bacteria in the mesenteric lymph nodes as recognized pathobionts genera (**Fig. 6E**). In addition,
494 16S rRNA sequencing performed 24 hours post-bowel preparation showed that most of the
495 bacterial taxa that translocated also increased in relative abundance in the feces, suggesting a
496 competitive advantage (**Fig. 6F**). These results indicate that, similar to *Salmonella* Typhimurium,
497 potential pathobionts can take advantage of the disruption caused by bowel preparation to
498 expand in the gut and even invade extraintestinal organs.

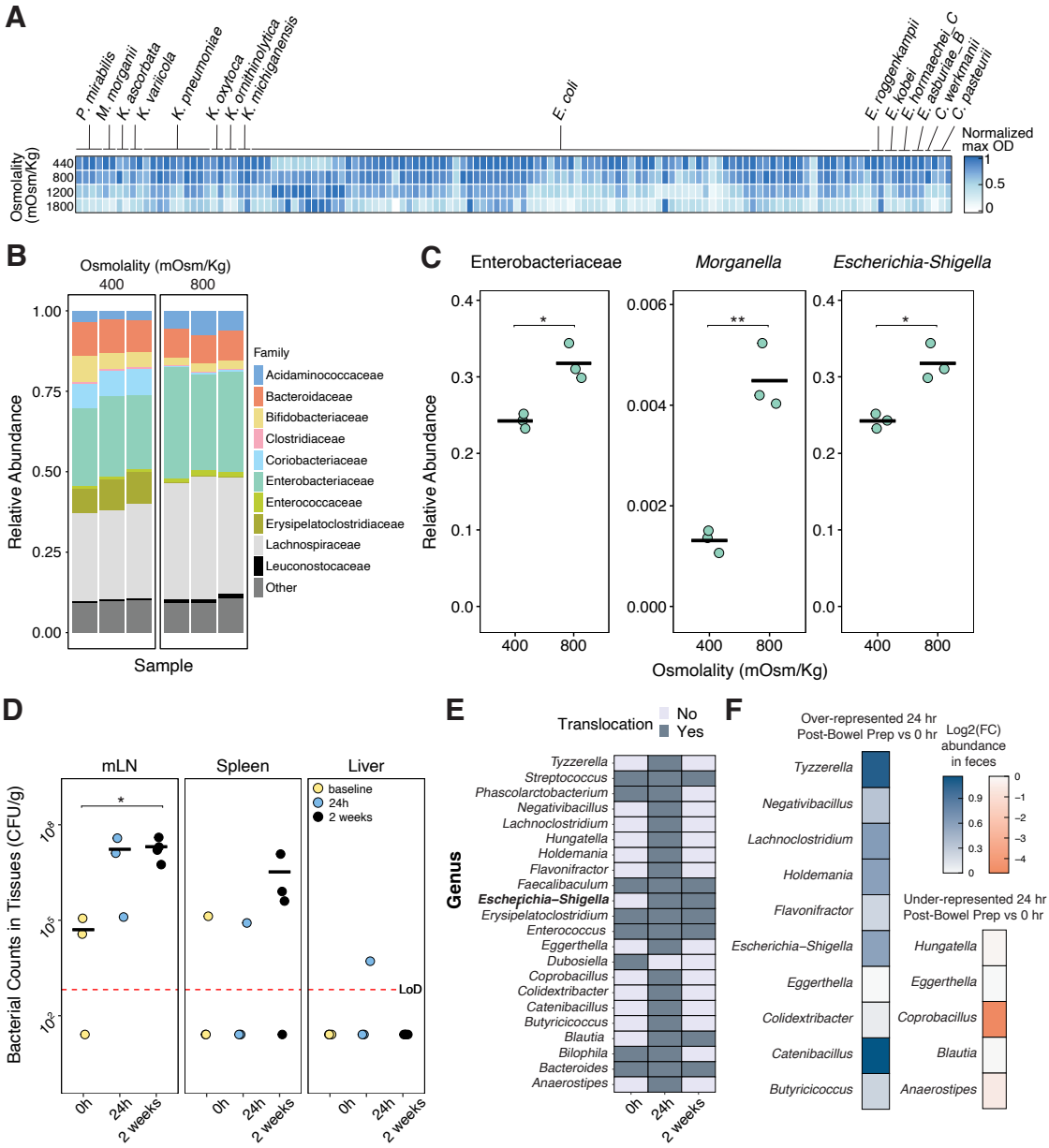

Figure 6. Potential pathobionts from patients with inflammatory bowel disease are resilient to osmotic perturbation *in vitro* and can translocate and persist in the mesenteric lymph nodes of germ-free mice after bowel preparation with a detergent laxative (polyethylene glycol, PEG). (A) Many of the 130 potential pathobionts isolated from patients with ulcerative colitis and cultured under anaerobic conditions were able to grow at osmotic stress levels meeting or exceeding those found in the mouse gut after bowel preparation (~750 mOsm/Kg). Normalized carrying capacity was measured at maximum OD600 after bacteria were cultured under aerobic conditions for 24 hours, and cultures were grown at 400, 800, 1200, and 1800 mOsm/Kg, adjusted with NaCl. (B) When a fecal sample obtained from an individual with ulcerative colitis was cultured under osmotic stress levels simulating normal (400 mOsm/Kg) and bowel prep, polyethylene glycol (PEG)-treated (800 mOsm/Kg) conditions in the mouse gut, 16S rRNA sequence data showed a shift in community composition under the high osmotic stress

conditions, including increased abundance of the family Enterobacteriaceae (genera *Morganella* and *Escherichia-Shigella*). (C) Significant increases in the relative abundance of the Enterobacteriaceae family and the genera *Morganella* and *Escherichia-Shigella* from (B) were observed (each osmolality *n*=3). Differences between treatment groups were analyzed with t-tests. (D) Significant levels of bacterial translocation from the gut to the mesenteric lymph nodes (mLN) but not the spleen and liver were observed after humanized germ-free Swiss Webster mice were inoculated with the same fecal sample from a patient with ulcerative colitis used in (B). Differences between post-bowel prep-treatment timepoints were analyzed with Kruskal-Wallis followed by Dunn's post-hoc test. (E) Translocating bacteria from (D) identified by 16S rRNA sequencing of the mLN show presence of potential pathobiont species (baseline *n*=3, 24h *n*=3, 2 weeks *n*=4). (F) A heat map of the abundance of taxa from (E) in mouse fecal samples collected 24 hours post-PEG treatment shows that most of the bacterial taxa that translocated also increased in relative abundance in the feces. LoD, limit of detection. $p > 0.05$; ns (not significant, not shown), $p < 0.05$; *, $p < 0.01$; **, $p < 0.001$; ***, $p < 0.0001$; ****.

Discussion

In this study, we set out to use *in vitro* and mouse models of bowel preparation to determine whether the procedure increases the gut's vulnerability to colonization by pathogens. We showed that (1) bowel preparation with PEG alters the intestinal environment and that (2) it can eliminate the natural microbiota's protection against *Salmonella* Typhimurium invasion (**Fig. 2**). In fact, after bowel preparation, even non-motile *Salmonella* Typhimurium could colonize the mouse gut and infect extra-intestinal organs, indicating that the stripping of the gut mucus layer during bowel preparation dramatically reduces the normal barriers to infection (**Fig. 4**). These findings in mice were supported by findings from a gut-on-a-chip model that mimicked the human gut; simulation of the conditions present in the gut after bowel preparation increased permeability of the gut epithelium and allowed *Salmonella* Typhimurium to translocate from the luminal side to past the endothelial layer (**Fig. 5D,E**). Finally, in germ-free mice inoculated with fecal samples from individuals with and without inflammatory bowel disease and then treated with PEG, we observed translocation of bacteria recognized as pathobionts from the gut to mesenteric lymph nodes (**Fig. 6**). Our findings show that bowel preparation reduces the gut microbiota's natural resistance to pathogens through multiple mechanisms, including increased levels of osmotic stress, depletion of the mucus layer, and reduced competition by commensal bacteria.

Our data indicate that shortly after bowel preparation is performed, before the commensal microbiota and gut environment have a chance to recover, hosts are extremely vulnerable to pathogens. In this study, a *Salmonella* Typhimurium inoculation dose as low as 1,000 bacteria was able to successfully colonize and expand within the guts of mice that had received PEG treatment 6 hours earlier, and even translocate to the lymph nodes, spleen, and liver (**Fig. 2G,H**). This dose is between ten thousand and a million times lower the usual dose used in the streptomycin models of *Salmonella* Typhimurium infection[37]. This expansion occurred despite the absence of bicarbonate treatment, which is commonly used to ensure the *Salmonella* Typhimurium load is not negatively affected by stomach acidity[38], or pretreatment with antibiotics[22,23].

Our data from mice suggest that the microbiota depletion is a key factor in the gut's increased susceptibility to pathogens after bowel preparation. After 24 hours, osmolality and mucus had recovered, but SCFA levels remained depleted—and *Salmonella* Typhimurium was still able to

558 colonize the gut (**Fig. 3F-H**). Butyrate, in particular, has been shown to improve the integrity of
559 the epithelial barrier and suppress excessive inflammation[27]. Importantly, higher SCFA levels have
560 been linked to lower *Salmonella* burdens in chickens[27] and to modulation of pathogen virulence.
561 Specifically, *in vitro* experiments demonstrated that exposure to butyrate downregulated
562 *Salmonella pathogenicity island 1* expression, decreasing epithelial invasion[39,40]. With intestinal
563 butyrate levels reduced due to bowel preparation, *Salmonella* Typhimurium may be less inhibited
564 and better able to invade tissue and translocate to extra-intestinal organs.
565
566 However, the highest levels of *Salmonella* Typhimurium colonization occurred 6 hours after bowel
567 preparation, when the mucus layer was at its thinnest (**Fig. 3B**). These findings align with previous
568 work in mice and humans with ulcerative colitis showing that thinning of the intestinal mucus
569 layer enhances bacterial penetration of the gut epithelium and increases host susceptibility to
570 pathogen infection[28,41]. Moreover, mice genetically engineered to lack intestinal mucus (*Muc2* -/-
571) display increased susceptibility to *Citrobacter rodentium*[42] as well as *Salmonella* Typhimurium[43].
572 Interestingly, although mucus loss occurred throughout the mouse digestive tract, we found
573 *Salmonella* Typhimurium infected cecal tissues and no pathology was observed in the colon (**Fig.**
574 **2E,F**). While a previous study suggested the cecum is the preferred side of *Salmonella*
575 Typhimurium infection due to incomplete mucus coverage[31], our findings suggest that the
576 mechanical changes induced by bowel preparation, particularly the thinning of the cecal mucosa,
577 may further enhance tissue invasion at this location, even in the absence of mucus throughout the
578 gut. Supporting this, a recent study has found that hypertonic stimulation increases bacterial
579 adhesion to host cells *in vitro*[44].
580
581 In contrast, streptomycin-treated mice exhibited pathology in both the cecum and colon (**Fig. S2**).
582 Notably, the mucus layer has been found to not be depleted following streptomycin treatment[45],
583 indicating that the presence of mucus is not the most critical factor limiting wild-type *Salmonella*
584 Typhimurium infection. Altogether, these findings highlight that while both mucus loss and SCFA
585 depletion contribute to increased *Salmonella* Typhimurium susceptibility, additional factors
586 unique to bowel preparation, such as increased osmolality and changed cecal tissue properties (**Fig.**
587 **1**) play a significant role in shaping pathogen colonization and invasion.
588
589 Normally, *Salmonella* Typhimurium needs a functioning flagellum to colonize the mammalian GI
590 tract[38], and previous studies have reported that disruption of *Salmonella* Typhimurium motility
591 reduces pathogen fitness and invasiveness *in vitro* and *in vivo*[46–48]. However, in absence of mucus,
592 after mice underwent bowel preparation, the non-motile *Salmonella* Typhimurium *ΔflhD* mutant
593 was able to colonize the guts of these mice and translocate to the mesenteric lymph nodes (**Fig.**
594 **4C)**. As the FlhD protein, which is a master regulator of flagellar biogenesis and motility, is
595 involved in coordinating virulence[49,50], the ability of *Salmonella* Typhimurium *ΔflhD* to
596 translocate suggests other virulence factors may facilitate *Salmonella* Typhimurium translocation
597 after bowel preparation. Specifically, type III secretion system (T3SS) pathogenicity islands (SPI-
598 1-3) are independent of the FlhD master regulator and enable *Salmonella* Typhimurium to
599 colonize, invade, and survive in the host without requiring motility[51,52]. This finding expands our
600 understanding of pathogen-host interactions in disrupted gut environments and suggests that also
601 non-motile pathogens may be able to exploit these conditions to invade the gut mucosa.
602

603 Our mouse data further suggest that the effects of bowel preparation on host susceptibility to gut
604 pathogens occur rapidly, and the host does not mount a strong response to it within that
605 timeframe (**Fig. 5A**). We observed only minor differences in cecal mucosa gene expression 6
606 hours after bowel preparation, when susceptibility to pathogens was at its peak. This suggests
607 host cells are not well adapted to respond to this perturbation within the timescale of peak
608 vulnerability to pathogen invasion. Other perturbations are known to lead to host epithelial
609 transcriptional responses on similar or faster timescales, for example, in the case of infection
610 upregulation of innate immune responses such as oxidative phosphorylation occurs within 8
611 hours[53], and natural circadian rhythms lead to changes in expression within less than 4 hours[54].
612
613 Our data from the gut-on-a-chip microfluidic system support the idea that the mouse findings
614 that bowel preparation increases gut epithelium permeability and pathogen translocation apply in
615 the context of the human gut epithelium as well, demonstrating the high barrier integrity and
616 relevance of the system (**Fig. 5B-E**). Within 4 hours of *Salmonella* Typhimurium challenge, we
617 observed a significant difference in paracellular permeability between bowel prep- and vehicle-
618 treated chips. This suggests that bowel preparation rapidly reduces epithelial integrity, increasing
619 permeability. Our gut-on-a-chip model employed Caco-2 and HT-29 cells to simulate the human
620 gut epithelium. In these cell types, PEG has been shown to have a some effect on the viability of
621 Caco-2 cells in culture (with ~20% decrease in viability at 5 and 10 mM after 5 days of PEG)[55].
622 Furthermore, PEG has been shown to decrease HT-29 cell viability and growth within a day of
623 culturing, inducing structural changes such as cell shrinking and chromatin condensing[55]. In the
624 case of bowel preparation, the concentration used is closer to 50 mM, although the perturbation
625 is shorter in time span. These data support the negative impact of PEG that may increase
626 susceptibility to pathogen infection. With regard to pathogen translocation, in a previous study
627 using the gut-on-a-chip system with mouse colon organoids, epithelial detachment was observed
628 15 hours after *Salmonella* Typhimurium challenge[56]; the faster timescales observed in our model
629 suggest that PEG and *Salmonella* have an additive effect to disrupt the epithelium.
630
631 Finally, we found that, unlike commensal bacteria, which display limited resilience to increased
632 osmolality[18], pathobionts common in patients with IBD are highly resilient to the osmotic
633 perturbation present after bowel preparation (**Fig. 6A**). Our mouse data suggest they can expand
634 and translocate effectively in the gut after bowel preparation (**Fig. 6D-F**). These results support
635 clinical findings of negative outcomes post bowel preparation in some patients with IBD[10–15] and
636 suggest that patients harboring osmolality-resilient pathobionts may be susceptible to exacerbation
637 of symptoms post procedure.
638
639 This study has several important limitations. Primarily, differences in gut physiology and
640 microbiota composition between humans and mice could limit the application of our findings from
641 mice to humans. Specifically, considerations such as transit time, size and physiology of the
642 digestive tract will have an impact on the windows of susceptibility to pathogens in humans vs
643 mice. However, given the similarity of our model to clinical bowel preparation (PEG laxative,
644 removal of intestinal contents) and the support of our findings in a human gut-on-a-chip system,
645 we believe our findings to be applicable. Future studies of bowel preparation in humans should
646 investigate the presence of specific pathobionts in biopsies. Importantly, previous findings already
647 highlight the increased representation of potential pathobionts members in the Enterobacteriaceae

family such as *E. coli* and *Klebsiella* in IBD biopsies[57–59]. However, the presence of these genera, alongside a characterization of their potential ability to act as a pathobiont (for example via the presence of toxin genes) need to be correlated to health outcomes of the patients beyond the diagnosis at the time of colonoscopy. Still, particularly because of the technical challenges of measuring bacterial translocation in humans[10–15], this animal model may provide important insights into which bacteria should be monitored in patients requiring more frequent colonoscopies, including those with IBD.

Similarly, differences between our gut-on-a-chip model and the actual human gut may limit application of findings from this study system. However, in the bowel prep system, due to the much-reduced microbiota and mucus layer following the laxative treatment, this model is particularly apt to model pathogen infection. Furthermore, enterocyte-like Caco-2 and goblet cell–like HT-29 co-cultures are a well-established, in-vivo-like model of the intestinal epithelium incorporating dynamic flow, sheer stress, and functional epithelial barriers[34,60,61]. Moreover, the average apparent permeability of our chips prior to infection was similar to those reported in the existing literature, including for studies that used the same type of chip in combination with human intestinal organoids from healthy donors (within the 10^{-7} P_{app} range)[62]. Taken together, while our study systems have inherent limitations, their ability to mimic key aspects of bowel preparation and pathogen susceptibility supports their utility in exploring the mechanisms underlying microbial translocation and infection.

In conclusion, our study establishes that, in both mouse and gut-on-a-chip models, bowel preparation rapidly alters the gut environment, making it more susceptible to colonization by both *Salmonella* Typhimurium, including a non-motile mutant that is normally unable to invade the gut, and pathobionts collected from patients with ulcerative colitis. In addition, gut preparation promotes the translocation of these bacteria from the gut to extraintestinal organs, such as nearby lymph nodes, the liver, and spleen. These findings suggest that gut preparation may have clinical implications that are not currently appreciated. Moreover, our findings suggest that other conditions that cause bouts of osmotic diarrhea, such as malabsorption, could promote the growth of pathobionts that harm health. Future research should focus on clarifying the effects of bowel preparation on gut health, especially in patients with conditions such as IBD that make them particularly vulnerable. By better understanding the specific changes induced by bowel preparation, as well as their associated risks, we can develop strategies to mitigate negative effects. For example, future studies could explore strategies such as modifications to bowel preparation formulations in order to protect the mucosal surface of the gut.

Resource Availability

Lead Contact

Carolina Tropini (carolina.tropini@ubc.ca)

Acknowledgments

The authors acknowledge that the land we performed this research on is the traditional, ancestral, and unceded territory of the xwməθkwəy̓əm (Musqueam) Nation. The land our laboratory is situated on has always been a place of learning for the Musqueam people, who for millennia have passed on in their culture, history, and traditions from one generation to the next on this site. We

encourage others to learn more about the native lands in which they live and work at https://native-land.ca/.

The authors thank Denise Monack and members of the Tropini Lab for useful conversations and insight, in particular Michael Hunter for critically reading the manuscript and Angele Arrieta for ordering supplies and managing lab processes. We acknowledge the University of British Columbia Centre for Disease Modeling and Natalia Carranza Garcia for support with animal work. We thank Ben Swenor and William Bralower from Emulate for answering questions and helping us get started on gut-on-a-chip experiments. This study also received support from the Life Sciences Institute Biofactorial High-Throughput Biology Core, supported by the University of British Columbia Global Research Excellence Biological Resilience Initiative. We thank Wanyin Deng and the Finlay lab for providing *Salmonella* Typhimurium strains. We thank Harper Health & Science Communications, LLC for editorial support. The authors acknowledge support from the Canadian Institute for Advanced Research / Humans and the Microbiome (FL-001253 Appt 3362, to C.T.), Michael Smith Foundation for Health Research Scholar Award (18239, to C.T.), Canada Foundation for Innovation / Infrastructure Operating Fund (38277), Canada Tier 2 Research Chair, Quantitative Microbiota Biology for Health Applications (CRC-2022-00036, to C.T.), Canadian Institutes of Health Research (CIHR) Project grant (PJT 191743), Crohn's and Colitis Canada / Grants In Aid of Research (625155), Paul Allen Foundation / Allen Distinguished Investigators (ADI) Program (12935, to C.T. and S.R.S.), and the CH.I.L.D Foundation Chair in Pediatric Gastroenterology (to B.A.V.).

Supplementary Figures

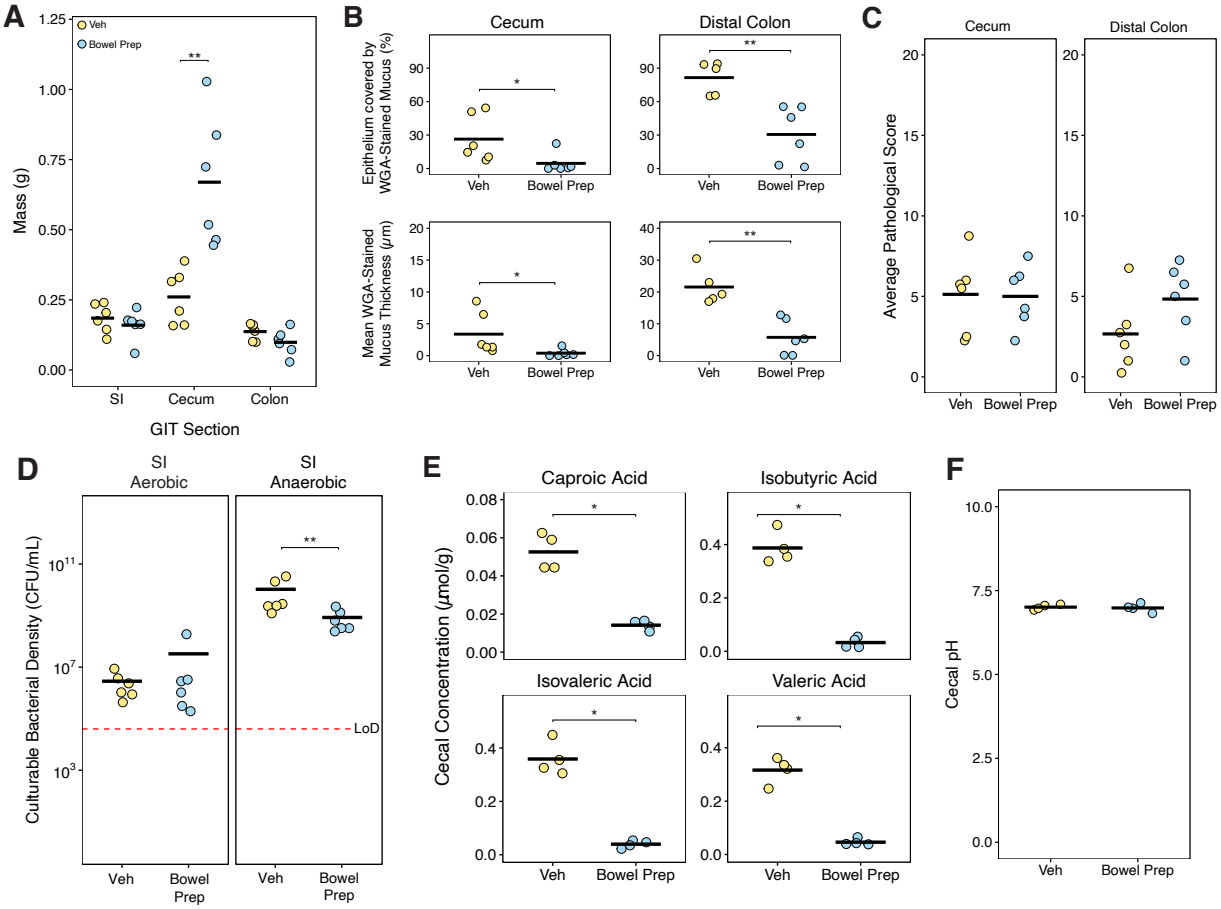

Supplemental Figure 1. Bowel preparation with a detergent laxative (polyethylene glycol, PEG) does not lead to overt pathology in the mouse gut at 6 hours post procedure, despite changes in cecal mass, mucus layer thickness, and short-chain fatty acid (SCFA) levels.
(A) The mass of the cecum, but not the small intestine or colon, was significantly higher in bowel prep- vs vehicle-treated mice (Veh *n*=6, Bowel Prep *n*=6). (B) Mucus coverage (*top*) and mucus layer thickness (*bottom*) were significantly higher in vehicle- vs bowel prep-treated mice, in both the cecum and distal colon (Veh *n*=6, Bowel Prep *n*=6). Both measures were quantified using WGA lectin staining to identify mucus. (C) Average pathological scores of the cecum and distal colon did not differ between bowel prep- and vehicle-treated mice (Veh *n*=6, Bowel Prep *n*=6). (D) Bacterial loads in the small intestine (SI), as measured by culture, did not differ between bowel prep- and vehicle-treated mice under aerobic conditions, but were significantly lower in bowel prep- vs vehicle-treated mice under anaerobic conditions (Veh *n*=6, Bowel Prep *n*=6). (E) The abundance of four SCFAs in the cecum was significantly lower in bowel prep- vs vehicle-treated mice (Veh *n*=4, Bowel Prep *n*=4). (F) Cecal pH did not differ between bowel prep- and vehicle-treated mice (Veh *n*=4, Bowel Prep *n*=4). **Statistics**: All differences between treatment groups were analyzed using a Wilcoxon ranked-sum test. $p > 0.05$; ns (not significant, not shown), $p < 0.05$; *, $p < 0.01$; **, $p < 0.001$; ***, $p < 0.0001$; ****.

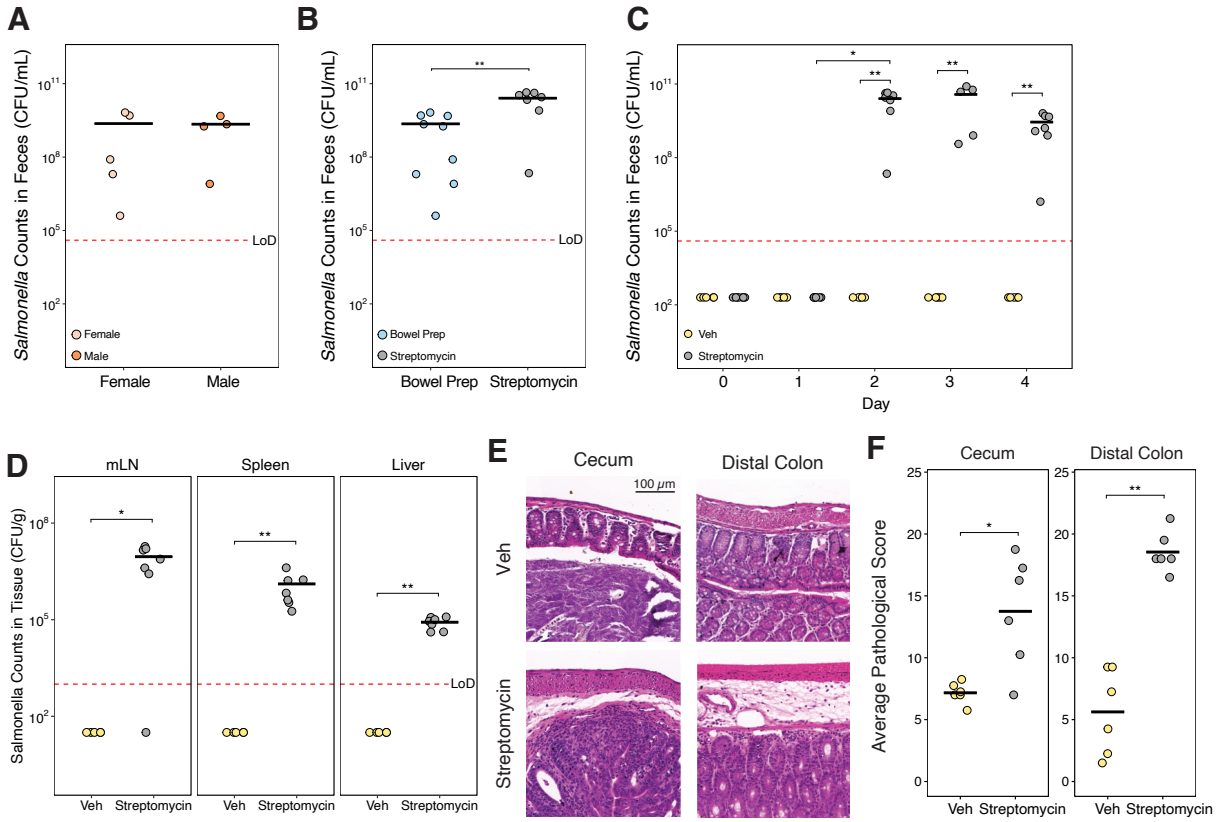

Supplemental Figure 2. Comparison of two mouse models of *Salmonella enterica* serovar Typhimurium—pre-treatment with bowel preparation (using the laxative detergent polyethylene glycol, PEG) or streptomycin—shows high levels of *Salmonella* Typhimurium burdens and robust translocation.

(A) One (not shown) and three days after inoculation, fecal *Salmonella* Typhimurium levels did not differ between bowel prep-treated male and female mice (Female *n*=5, Male *n*=4). Differences between treatment groups were analyzed using a Wilcoxon ranked-sum test. (B) Six hours post bowel prep, *Salmonella* Typhimurium levels were significantly lower in the feces of bowel prep-treated mice (from **Fig. 2C**) vs streptomycin-treated mice (Bowel Prep *n*=9, Streptomycin *n*=7). Differences between treatment groups were analyzed using a Wilcoxon ranked-sum test. (C) Fecal *Salmonella* Typhimurium levels were significantly lower in the feces of vehicle- vs streptomycin-treated mice up to 4 days after inoculation (Veh *n*=5, Streptomycin *n*=7). Differences between timepoints were analyzed with a Wilcoxon ranked-sum test, and differences between Streptomycin samples were analyzed with a Friedman test followed by Nemenyi post-hoc test. (D) *Salmonella* Typhimurium translocation from the gut to the mesenteric lymph nodes (mLN), liver, and spleen were significantly higher in streptomycin- vs vehicle-treated mice 72 hours after inoculation (Veh *n*=5, Streptomycin *n*=7). Differences between treatment groups were analyzed using a Wilcoxon ranked-sum test. (E) H&E-stained sections of the cecum and distal colon in streptomycin- and vehicle-treated mice show pathology in streptomycin-treated mice 3 days after inoculation with *Salmonella* Typhimurium. (F) Histopathological scoring of the distal colon and cecum in streptomycin- and vehicle-treated mice show increased pathology in both cecum and distal colon at 3 days after inoculation with *Salmonella* Typhimurium (Veh *n*=6, Streptomycin *n*=6). Differences between treatment groups were analyzed using a Wilcoxon ranked-sum test. LoD, limit of detection. $p > 0.05$; ns (not significant, not shown), $p < 0.05$; *, $p < 0.01$; **, $p < 0.001$; ***, $p < 0.0001$; ****.

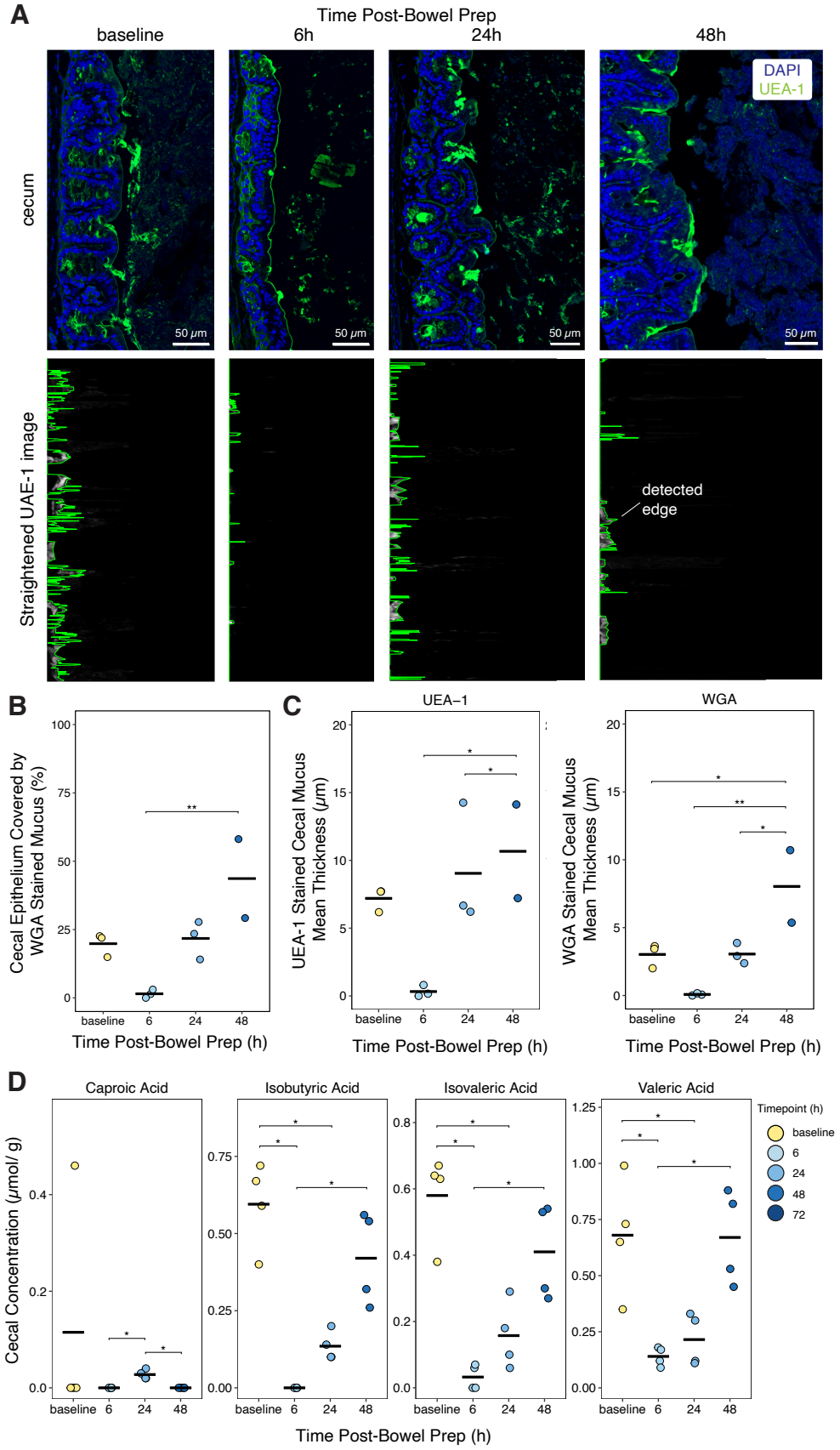
A
Time Post-Bowel Prep
baseline
6h
24h
48h
DAPI
UEA-1
cecum
50 μm
Straightened UAE-1 image
detected
edge
B
Cecal Epithelium Covered by
WGA Stained Mucus (%)
Time Post-Bowel Prep (h)
C
UEA–1
WGA
UEA-1 Stained Cecal Mucus
Mean Thickness (μm)
WGA Stained Cecal Mucus
Mean Thickness (μm)
D
Caproic Acid
Isobutyric Acid
Isovaleric Acid
Valeric Acid
Cecal Concentration (μmol/ g)
Timepoint (h)
baseline
6
24
48
72

Supplemental Figure 3. In the mouse cecum, short-chain fatty acid (SCFA) levels take longer to recover than the mucus layer after bowel preparation using the laxative detergent polyethylene glycol (PEG) .

(A) *Top*: Representative confocal images of the cecum stained with DAPI which indicates host DNA (*blue*) and UEA-1 which indicates mucus (*green*) show decreased mucus levels after PEG treatment, but recovery within 24 hours. *Bottom*: Representative UEA-1 channel images straightened relative to the epithelium to highlight the edge of the mucus layer, used to quantify mucus coverage and thickness. (B) Mucus coverage levels show recovery to baseline levels 24 hours after PEG treatment (baseline-24h n=3, 48h n=2). Differences between timepoints were analyzed using a one-way ANOVA with Tukey's post-hoc test for multiple comparisons. (C) Cecal mucus thickness measured using UEA-1 (*left*) and wheat germ agglutinin (WGA, *right*) staining show 24 hours after PEG treatment (baseline-24h n=3, 48h n=2). Differences between timepoints were analyzed using a one-way ANOVA with Tukey's post-hoc test for multiple comparisons. (D) The levels for three of four SCFAs tested remain depleted at least 24 hours after PEG treatment (each timepoint n=4). Differences between timepoints were analyzed with Kruskal-Wallis followed by Dunn's post-hoc test. $p > 0.05$; ns (not significant, not shown), $p < 0.05$; *, $p < 0.01$; **, $p < 0.001$; ***, $p < 0.0001$; ****.

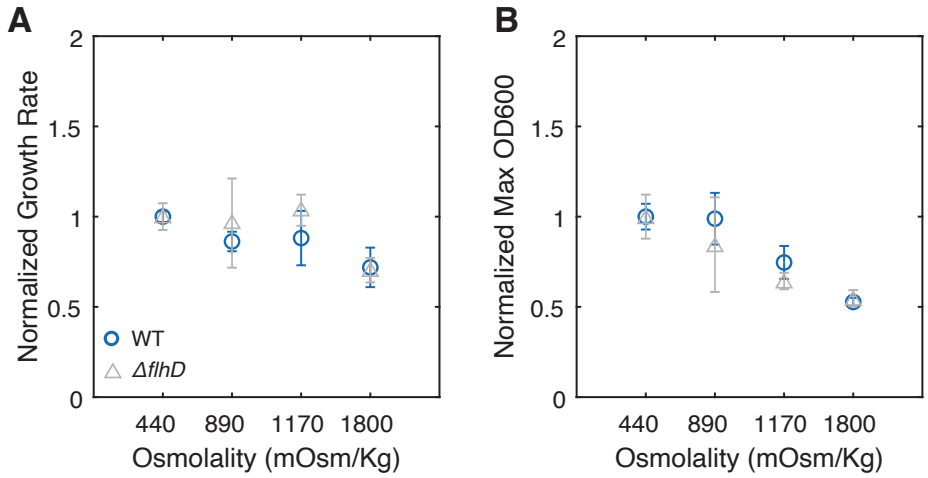

Supplemental Figure 4. In culture, growth of the *Salmonella enterica* serovar Typhimurium non-motile *ΔflhD* mutant is robust under high osmolality conditions.

(A) Normalized maximum growth rate and (B) normalized maximum optical density (OD600) of wild type and *ΔflhD Salmonella* Typhimurium are comparable in aerobic conditions and media of varying osmolalities, adjusted with polyethylene glycol (each osmolality & strain n=4). Differences between timepoints and strains were analyzed using a two-way ANOVA with Tukey's post-hoc test for multiple comparisons. $p > 0.05$; ns (not significant, not shown), $p < 0.05$; *, $p < 0.01$; **, $p < 0.001$; ***, $p < 0.0001$; ****.

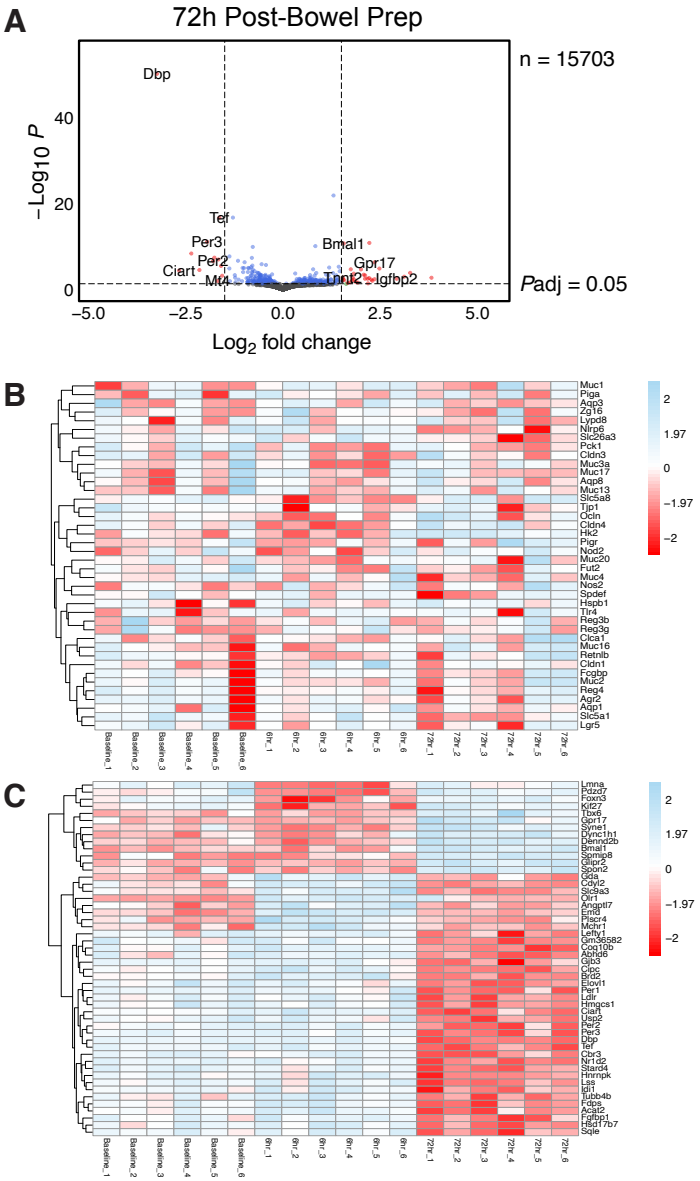

Supplemental Figure 5. In mice, the expression of circadian rhythm genes is significantly altered 72 hours after bowel preparation with the detergent laxative polyethylene glycol (PEG), but differences in expression of other genes is minimal at both 6 and 72 hours post treatment. (A) Volcano plot of differential gene expression in mouse cecal tissue at baseline and 72 hours after PEG treatment shows few genes were differentially expressed, including genes involves in gut mucus layer production. The plot shows the names of genes with adjusted p-values (Benjamin-Hochberg false discovery rate–corrected) <0.05 and Log_2 fold change >1.5. (B) Heat map of gene expression at 0, 6, and 72 hours after bowel prep-treatment of the mice from (A), for the top 50 differentially expressed genes by mean Z-score. The circadian rhythm genes *Dbp*, *Tef*, *Per2-3*, *Ciart* were all significantly downregulated at 72 hrs vs baseline, whereas *Nfil3* and *Bmal1* were upregulated over the same period. *Dbp* (D-box binding protein) regulates circadian gene expression and controls transcription of several clock-controlled genes, including *Tef* (thyrotroph embryonic factor), which also plays a role in circadian regulation[63]. *Per* genes (including *Per2* and *Per3*) are core components of the circadian clock that encode the PERIOD proteins, which usually accumulate in an animal's active phase (night for mice[64,65]) to help maintain the circadian rhythm[63,66]. *Nfil3*

(nuclear factor interleukin 3-regulated) represses *Dbp*, and *Bmal1* (Basic Helix-Loop-Helix ARNT Like 1) activates *Per* genes as part of the core transcriptional-translational feedback loop. Exceptions of genes that were significantly changed in expression at 6 hours compared to baseline included overexpression of genes involved in intestinal tumor proliferation, such as Chordin-like 2 (*chrdl2*)[67], prostate stem cell antigen (*psca*)[68], C-C chemokine 17 (*ccl17*)[69] and oxidized low-density lipoprotein receptor 1 (*olr1*)[70], as well as genes involved in ion transport or stress responses, such as the potassium voltage-gated channel subfamily E member 4 (*kcne4*)[71], cation transport regulator-like protein 1 (*chac1*)[72], and *Slc9* family of Na^+/H^+ exchangers (*slc9a3*, NHE3)[73]. Genes whose expression increased between the 6- and 72-hour timepoints included *hk2* (involved in metabolic response to stress[74]), *slc5a8* (an SCFA transporter[75]), and *cldn4* (a component of tight junction strands involved in paracellular permeability[76]). Genes whose expression decreased over this period included *nlrp6* (a member of the NOD-like receptor family and cytosolic innate immune sensor that recognizes microbe-associated molecular patterns[77]) and *slc26a3* (involved in response to hyperosmotic stress[78]).

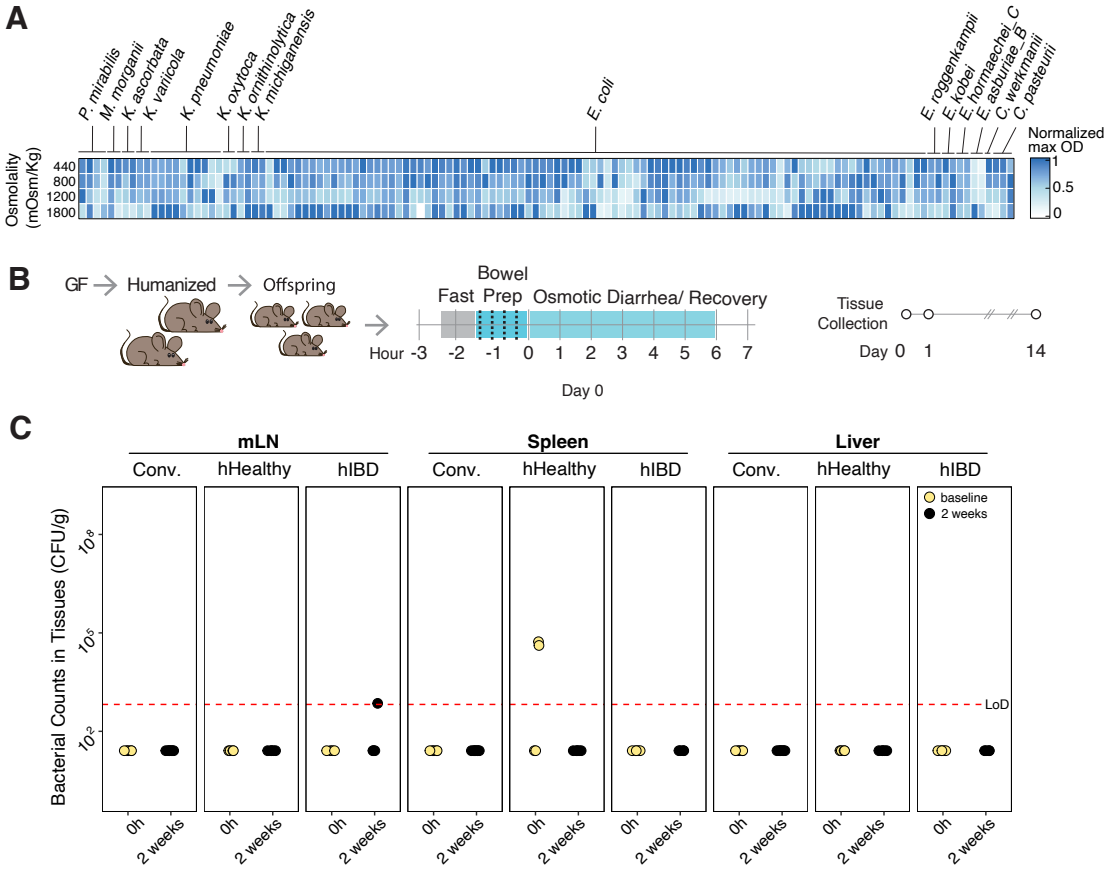

Supplemental Figure 6. In culture and a germ-free mouse model, pathobionts collected from patients with ulcerative colitis can grow at osmolality levels comparable to those present after bowel preparation with the detergent laxative polyethylene glycol (PEG).
(A) Many of the 130 potential pathobionts isolated from patients with ulcerative colitis and cultured under anaerobic conditions were able to grow at osmotic stress levels meeting or exceeding those found in the mouse gut after bowel preparation (800 mOsm/Kg). Normalized carrying capacity was measured at maximum OD600 after bacteria were cultured under anaerobic conditions for 24 hours, and cultures were

grown at 400, 800, 1200, and 1800 mOsm/Kg, adjusted with NaCl. (B) Schematic of germ-free (GF) mice humanized with a fecal sample from a patient with ulcerative colitis or a person without the condition, and then bred for experimental use. Mouse offspring 8-12 weeks of age were used in our experiments, and samples were collected over 2 weeks. (C) Anaerobic bacterial translocation measured in extraintestinal organs, mesenteric lymph nodes (mLN), spleen, and liver, at baseline, 24 hours, and 2 weeks post-bowel prep in conventional mice, healthy-humanized mice, and IBD-humanized mice after mice were treated with PEG shows no translocation in C57BL/6J mice (Conv. each tissue: baseline n=5, 2 weeks n=7. hHealthy each tissue: baseline n=4, 2 weeks n=5. hIBD mLN: baseline n=4, 2 weeks n=4. hIBD Spleen & Liver: baseline n=5, 2 weeks n=4.). Bacteria from the organs were cultured under anaerobic conditions. Differences between timepoints were analyzed with Kruskal-Wallis followed by Dunn's post-hoc test. Abbreviation: LoD, limit of detection. $p > 0.05$; ns (not significant, not shown), $p < 0.05$; *, $p < 0.01$; **, $p < 0.001$; ***, $p < 0.0001$; ****.

Supplemental Data Table S1. Mouse cecal RNA-seq data and statistics, refers to Fig. 5A. Host cecal tissue transcriptomics were performed at Baseline, 6 hours, and 72 hours post-bowel preparation and analyzed as referred to in the Methods. Description of sheets and columns can be found below.
Sheet "rna-seq-raw_counts": This table summarizes the raw gene expression counts from the extracted RNA.

- CC_1_S59ReadsPerGene.out.tab- CC_6_S64ReadsPerGene.out.tab: Raw gene expression counts under baseline conditions for mice 1–6.
- CC_7_S65ReadsPerGene.out.tab- CC_12_S70ReadsPerGene.out.tab: Raw gene expression counts at 6 hours post-treatment for mice 1–6.
- CC_13_S71ReadsPerGene.out.tab- CC_18_S76ReadsPerGene.out.tab: Raw gene expression counts at 72 hours post-treatment for mice 1–6.

Sheet "DESeq_lfc": This table summarizes the results table generated from the DESeq2 analyses as outlined in the methods.

- Gene: The official symbol for the gene.
- Description: A brief description of the gene's function or associated protein.
- Baseline_x: The average normalized counts, normalized by sequencing depth across all samples for mice1-6 under baseline conditions.
- 6hr_x: The average normalized counts, normalized by sequencing depth across all samples for mice 1-6 at 6 hours post treatment.
- 72hr_x: The average normalized counts, normalized by sequencing depth across all samples for mice 1-6 at 72 hours post treatment.
- Log2FoldChange_x: indicates how much the gene expression changed between the samples collected at 6 or 72 hours post- treatment and the samples collected at baseline. This value is reported on a log2 scale.
- lfcSE_x: The standard error estimate for the log2 fold change estimate for the samples collected at 6 hours or 72 hours post-treatments
- pvalue_x: P-value of the test for the gene for the samples collected 6 hours or 72 hours post-treatment
- padj_x: Adjusted P-value for multiple testing for the gene for the samples collected 6 hours or 72 hours post-treatment
- mean_Baseline, mean_6hr, mean_72hr: Mean normalized counts for each respective condition, averaged across all replicates.

Sheet "DESeq Z score": This table summarizes the Z-scores for transcriptomic analysis across multiple conditions and time points. The Z-score is the number of standard deviations away from the mean of the expression levels of a gene across all the samples.

- Gene: The official symbol for the gene.
- Description: A brief description of the gene's function or associated protein.
- Z_Baseline_x: Z-scores representing gene expression levels under baseline conditions for mice 1–6.
- Z_6hr_x: Z-scores for gene expression at 6 hours post-treatment for mice 1–6.
- Z_72hr_x: Z-scores for gene expression at 72 hours post-treatment for mice 1–6.
- Z_Baseline_mean, Z_6h_mean, Z_72h_mean: Mean Z-scores for each respective condition, averaged across all replicates.

Supplemental Data Table S2. Papp calculations, refers to Fig. 5D. Samples from all channels were collected at baseline, 4 hours post infection, and 24 hours post infection and analyzed as referred to in Methods. Description of the sheets can be found below.

Sheet "Papp_Calculator": This sheet is the template of the Emulate Papp calculator[79] used in other sheets.

Sheet "baseline": This sheet shows the Papp calculations for samples collected at baseline.

Sheet "4hpi": This sheet shows the Papp calculations for samples collected at 4 hours post infection.

Sheet "24hpi": This sheet shows the Papp calculations for samples collected at 24 hours post infection.

CRediT authorship contribution statement:

CAC: Conceptualization, Methodology, Formal Analysis, Investigation, Data Curation, Writing – original draft, Writing - Review & Editing, Visualization
GM: Methodology, Formal Analysis, Investigation, Writing - Review & Editing, Visualization
BDD: Methodology, Formal Analysis, Investigation, Writing - Review & Editing, Visualization
KN: Conceptualization, Methodology, Investigation, Writing - Review & Editing, Supervision
AS: Investigation, Formal Analysis
CS: Investigation
JH: Formal Analysis
DT: Investigation
IP: Formal Analysis
DMP: Investigation
TF: Investigation
SRS: Conceptualization, Resources, Supervision
MS: Resources, Supervision
BAV: Conceptualization, Resources
CT: Conceptualization, Resources, Writing – original draft, Writing– review & editing, Formal Analysis, Supervision, Project administration, Funding acquisition.

Declarations of interest: none

Methods

Animal Handling and Ethics

All animal experiments were conducted in accordance with the ethical guidelines of the University of British Columbia's (UBC) animal care procedures, following protocol number A23-0115 approved by the Animal Care Committee. C57BL/6J or (as noted) Swiss Webster male and female mice between 8-12 weeks of age were used and were provided with an autoclaved standard diet (Purina LabDiet 5K67). As we did not observe sex differences, male and female mice were analyzed together in all experiments. Experimental groups that underwent oral gavage were monitored at 1 hour and 24 hours post-procedure. Daily health checks for mortality after infection were performed, and mice were euthanized if they lost more than 20% of their body weight or displayed signs of distress. Euthanasia at indicated tissue-collection time points was performed using carbon dioxide asphyxiation followed by cervical dislocation. I

Bowel Preparation Mouse Model

Bowel prep solution was prepared by dissolving 42.5% (w/v) polyethylene glycol (PEG) (commercially branded Restoralax) in ddH_2O and filter sterilized. Food was withdrawn from all cages 1 hour before the bowel prep procedure. Mice were orally gavaged with 200 µL of bowel prep solution every 20 minutes a total of 4 times. Vehicle-treated mice were orally gavaged with 200 µL of water following the same dosing time as bowel prep-treated mice. Food and water were readministered after the procedure. Following bowel prep, we evaluated the impact of high dose osmotic laxatives on the gut environment and the gut microbiota at 6, 24, 48, and 72 hours post-bowel prep and compared to untreated controls sacrificed and the 6-hour timepoint (baseline).

To investigate the effects of bowel prep on the gut environment, we characterized a murine bowel preparation method previously used to facilitate the transplantation of human microbes into mice[80]. Mice with a conventional microbiota were fasted and then orally gavaged 4 times with PEG dissolved in water (bowel prep), while controls received water as the vehicle alone (Fig. 1A). Mice were euthanized six hours post-bowel prep, and intestinal tissues and contents were collected. Bowel prep-treated mice had an average cecal osmolality that was 1.8-fold higher than vehicle-treated controls (725 vs. 437 mOsm/Kg, $p < 0.001$) (Fig. 1B) and a higher cecal mass, indicative of osmotic diarrhea and increased luminal contents during bowel prep (Fig. S1A).

Cecal Osmolality and pH Measurements

Mice were sacrificed, and cecal contents were collected and placed on ice. The osmolality of the cecal contents was directly measured using an Advanced Instruments Osmo1 Single-Sample Micro-Osmometer (Fisher Scientific, 22-047-531). pH was measured with a calibrated micro pH probe (Orion PerpHecT ROSS Combination pH Micro Electrode, Catalog number: 8220BNWP).

Tissue Collection

Sterile tools were used to collect the lower lobe of the liver, mesenteric lymph nodes, and the spleen. The tissues were placed in pre-weighed sterile 2 mL tubes containing 200 µL of PBS and were put on ice. Cecal contents were collected, and half of the contents were flash-frozen on dry ice, while the other half was placed on ice for downstream analysis. The ileum, cecum, and colon tissues were collected in histology cassettes and immediately fixed in methacarn solution (60%

962 dry methanol (Fisher Chemical, A412P-4), 30% chloroform (Fisher Chemical, C298-500), 10%
963 glacial acetic acid (Fisher Chemical, A38-212)) for 7 to 14 days. The samples were then washed
964 twice in methanol for 30 minutes, twice in 100% ethanol (Sigma, P016EAAN) for 20 minutes, and
965 twice in xylenes (Fisher Chemical, X3P-1GAL) for 15 minutes. The tissues were coated and
966 incubated in paraffin at 60°C for 2 hours and then dried at room temperature. Paraffin blocks were
967 cut into 4 µm sections and mounted on slides by the British Columbia Children's Hospital
968 Research Institute's Histology Core[81].
969
970 **Lectin Staining of the GIT**
971 Paraffin was removed from sectioned slides through incubation at 60ºC for 10 minutes, followed
972 by 2 incubations in pre-warmed xylenes at 60ºC. Slides were then incubated in 99.5% ethanol for
973 5 minutes, then left to dry and circled with a PAP (liquid blocker) pen (Fisher Scientific)[81]. DAPI
974 (10 µg/mL, Sigma Aldrich), UEA-1 (Fluorescein-labeled Ulex Europaeus Agglutinin I, 40 µg/mL,
975 Vector Laboratories), and WGA (Rhodamine Red-X-labeled Wheat Germ Agglutinin, 30 µg/mL,
976 Vector Laboratories) were applied to fully cover the samples (approximately 250 µL) and
977 incubated in the dark at room temperature for 45 minutes (Table 1). The slides were then washed
978 in PBS 3 times. Sections were left to dry for 5 minutes, and ProLong Gold Antifade Mountant,
979 (Invitrogen, P10144), was applied, followed by a #1.5 glass coverslip[81]. Images were collected
980 using a Zeiss LSM 900 confocal microscope with the ZEN 2020 software. Mucus thickness was
981 quantified using the analysis platform BacSpace[82].
982
983 **Confocal Image Straightening and Mucus Quantification**
984 Confocal images of longitudinal sections of different organs (ileum, cecum, proximal and distal
985 colon) were processed using the BacSpace image analysis pipeline using MATLAB software[82].
986 Briefly, BacSpace identifies the epithelial boundary based on DAPI signal and straightens images
987 relative to the epithelium. To quantify inner mucus layer thickness, the steepest decrease in WGA
988 or UEA-1 signal between two user-defined coordinates along the x-axis of straightened images
989 (corresponding to two distances from the epithelium) was identified at each position along the
990 epithelium. Distance from this boundary to the epithelial edge was defined as thickness of the inner
991 mucus layer at a given point along the epithelium. The average thickness of two sections from 3
992 different mice were calculated in every organ. To calculate mucus coverage, the ratio of epithelial
993 segments with non-zero mucus layer values to those with detected mucus was calculated.
994 Differences in average thickness between treatment and control groups (Fig. 1) or between
995 timepoints post-bowel prep (Fig. 3) were assessed using a one-way ANOVA.
996
997 **Hematoxylin & Eosin Tissue Histology**
998 Paraffin was melted from the section slides by heating the slides in coplin jars at 60°C for 10
999 minutes. Slides were then incubated in the coplin jars in 60 ºC xylenes for 3 minutes twice followed
1000 by 2 incubations in 100% EtOH for 2 minutes each, 95% EtOH for 2 minutes, and in ddH20 for 2
1001 minutes[83]. Next, the hematoxylin stain was performed by filling the coplin jars with Hematoxylin
1002 Solution, Gill's No. 2 (Sigma Aldrich, GHS216), and incubating for 3 minutes, then in ddH_2O for
1003 1 minute, differentiator solution (0.3% v/v 10N HCl [Fisher Chemical, SA49], 70% v/v EtOH
1004 [Sigma, P016EAAN] in ddH2O)) for 30 seconds, ddH20 for 1 minute, and blueing reagent (0.2%
1005 w/v $NaHCO_3$ [Fisher BioReagents, BP328-500], 4.1% w/v $MgSO_4 \cdot 6H_2O$ [Fisher BioReagents,
1006 BP213-1] in ddH2O)) for 1 minute. For the Eosin stain, slides remained in the coplin jar and were

1007 filled with 95% EtOH for 1 minute followed by Eosin Y solution (Sigma Aldrich, HT110116), for
1008 45 seconds. The stain was followed by washes in 95% EtOH for 1 minute, in 100% EtOH for 1
1009 minute 3 times, and in xylenes for 2 minutes twice. Stained slides were mounted using Permount
1010 (Fisher Chemical, SP15-100), a xylene-based mounting medium, and allowed to solidify for at
1011 least 24 hours[83]. H&E images were acquired using the 3D HISTECH Slide Scanner at 37x.
1012
1013 **Pathology Scoring**
1014 H&E-stained sections of the cecum and distal colon were assessed for pathology in the lumen,
1015 epithelium, mucosa, and submucosa of the gut. Luminal pathology was scored based on the
1016 presence of necrotic epithelial cells and polymorphonuclear neutrophils (PMNs) (0 = none, 1 =
1017 scant, 2 = moderate, 3 = dense). The epithelium was scored for desquamation (0 = no change, 1 =
1018 limited shedding, 2 = moderate shedding per lesion), regenerative change (0 = none, 1 = mild, 2 =
1019 moderate, 3 = severe), ulceration (1 = epithelial ulceration), and PMNs in the epithelium (1 =
1020 PMNs present). The mucosa was scored based on crypt abscesses (0 = none, 1 = mild, 2 =
1021 moderate, 3 = severe) and the presence of mucin plugs and granulation tissue (1 = present). Lastly,
1022 the submucosa was scored for edema, mononuclear cell infiltration, and PMN infiltration (0 = no
1023 change, 1 = mild, 2 = moderate, 3 = severe). Scores for each location across the image were
1024 summed together, with the maximum pathological score being 24 per image. Images were scored
1025 by two blinded scorers, and the scores were averaged for each image.
1026
1027 **Mucosa Thickness Measurements**
1028 20X images of H&E-stained tissues were exported in TIFF format from SlideViewer. TIFF images
1029 were converted from RGB to 8-bit format in FIJI, and pixel values were inverted so that tissues
1030 appeared light against a dark background. BacSpace was used to create two masks; one mask
1031 outlined the submucosal edge of the mucosa, and the other mask outlined the luminal edge of the
1032 epithelium. Both masks were applied to the original image so that only the mucosa and epithelium
1033 were non-zero values. BacSpace was then used on the masked images to straighten the image
1034 relative to the luminal edge of the epithelium. The luminal edge of the epithelium in the
1035 straightened image was detected as the greatest decrease in signal along the x-axis of the
1036 straightened image at each point along the epithelium. The mean thickness was quantified for each
1037 image, and the mean thicknesses of two images from the cecum and two images from the distal
1038 colon from three different mice per treatment (total = 6 images per treatment per organ) were
1039 compared using a Wilcoxon rank test.
1040
1041 **Quantification of Bacterial Levels in Feces**
1042 1 μL of feces was diluted in 200 μL of sterile PBS. The solution was serially diluted at 1:10 down
1043 a 96-well plate. Next, 5 μL fecal dilutions were spot-plated on both LB-streptomycin agar plates
1044 and Columbia Blood agar plates. Plates were incubated aerobically overnight at 37 ºC. Single
1045 colonies were counted from the highest possible dilution and back calculated to determine the
1046 absolute microbial abundance.
1047
1048 **DNA Extraction, Library Preparation, 16S rRNA Sequencing and Analysis**
1049 DNA was extracted from fecal pellets and cecal contents using the DNeasy 96 PowerSoil Pro
1050 QIAcube HT Kit (Qiagen Inc., Valencia, CA) according to the manufacturer's instructions.
1051

1052 For all 16S rRNA runs except for the *in vitro* IBD (**Fig. 6B,C**), 16S rRNA library preparation was
1053 conducted at the Biofactorial High-Throughput Biology (Bio!) Facility at the University of British
1054 Columbia. Amplification of the V4 region was performed with 515F/926R primers (515F, 5'-
1055 GTGYCAGCMGCCGCGGTAA-3'; 926R, 5'-CCGYCAATTYMTTTRAGTTT-3'). Pooled
1056 libraries were then submitted to the Bio! facility, where sequencing was performed on the Illumina
1057 MiSeq™ platform with v2 2 x 300 bp paired-end read chemistry. For the *in vitro* IBD samples,
1058 16S library preparation was performed by Gut4Health as previously described[84]. Amplicons of the
1059 V4 region of the 16S rRNA were generated using KAPA HiFi HotStart Real-time PCR Master
1060 Mix (Roche) and barcode primers 515F: GTGYCAGCMGCCGCGGTAA and 806R:
1061 GGACTACNVGGGTWTCTAAT. Purified PCR libraries were normalized and pooled with the
1062 SequalPrepTM normalization plate (Applied Biosystems). Library concentrations were confirmed
1063 using the QubitTM dsDNA high sensitivity assay kit (Invitrogen) and KAPA Library
1064 Quantification Kit (Roche). The purified pooled libraries were then submitted to UBC's
1065 Bioinformatics and Sequencing Consortium (SBC). Paired end read sequencing was carried out
1066 either on the Illumina MiSeqTM v3 platform with 2 x 300 bp paired end-read chemistry or the
1067 NextSeq 600 cycle P1 with 2 x 301 bp. To ensure DNA quality and quantity, an Agilent high
1068 sensitivity DNA kit (Agilent) was employed on an Agilent 2100 Bioanalyzer.

1069 Read quality was assessed by running FASTQC[85] on the generated FASTQ files. Reads were then
1070 imported into QIIME2-2023.9 for subsequent analyses[86]. DADA2 (via q2-dada2) was used to
1071 denoise and quality filter the data; then reads were trimmed to remove primer sequences while
1072 maintaining mean Phred quality scores >Q30[87]. Using the QIIME classification plugin (q2-feature-
1073 classifier), amplicon sequence variants (ASVs) were classified via a naïve Bayes machine-learning
1074 taxonomic classifier against the SILVA 138 99% identity reference sequence database[88]. Multiple
1075 sequence alignment and phylogenetic tree generation was performed using MAFFT (via q2-
1076 alignment) and FastTree2 respectively (via q2-phylogeny)[89,90]. Plotting was conducted using R
1077 v4.2.2[91]. Tidyverse[92] and ggplot2[93] packages were used for data visualization. The packages
1078 phyloseq[94], ggpubr[95], and vegan[96] were used for sample rarefaction, calculation, and visualization
1079 of alpha and beta diversity metrics.

1080 **SCFA Extraction from Cecal Contents**
1081 SCFAs were extracted from 40 to 100 mg of flash-frozen cecal contents. The samples were
1082 homogenized with 0.8 mL of 25% phosphoric acid (LabChem) and centrifuged at 15,000 × g for
1083 10 minutes at 4°C. The supernatant was removed from all samples and centrifuged again.
1084 Subsequently, 800 µL of the supernatant was filtered through a 0.45 µm filter (Fisher) and mixed
1085 with 0.2 mL of the internal standard solution containing 24.5 mmol/L isocaproic acid in a GC vial
1086 (12 × 32mm, Thermo Scientific). SCFAs were quantified by gas chromatography-mass
1087 spectrometry by the AFNS Chromatography Facility at the University of Alberta, as previously
1088 described[97].
1089
1090 ***Salmonella* Typhimurium Culture and Inoculum Preparation**
1091 *Salmonella* Typhimurium *ΔflhD* was a gift from the Finlay Lab, UBC. Glycerol stocks of the
1092 naturally streptomycin resistant *Salmonella enterica* Typhimurium SL1344 strains (*Salmonella*
1093 Typhimurium (WT) and *Salmonella* Typhimurium *ΔflhD*) were streaked onto Luria-Bertani Miller
1094 (LB) 1.5% agar plates supplemented with streptomycin (100 µg/mL). Following incubation at

1095 37°C for 24 hours without agitation, a single *Salmonella* Typhimurium colony was selected from
1096 the agar plate and transferred to 5 mL of LB liquid broth containing 100 µg/mL streptomycin. The
1097 culture was then aerobically incubated at 37°C with shaking at 200 rpm for 17 hours. Subsequently,
1098 the cultures were serially diluted in PBS to achieve the desired inoculant bacterial counts.
1099
1100 ***Salmonella* Typhimurium Osmolality Growth Measurements**
1101 Wildtype *Salmonella* Typhimurium or *Salmonella* Typhimurium *ΔflhD* were diluted 1:100 from
1102 overnight LB cultures in fresh LB media adjusted to ~400, 800, 1200, and 1800 mOsm/Kg using
1103 PEG (Restoralax). Growth curves were obtained using a Biotek Synergy H1 plate reader at 37°C
1104 for 24 hours aerobically. The plates were shaken orbitally every 15 minutes following the
1105 collection of OD600 measurements. Background absorbance subtraction was performed from non-
1106 inoculated wells. The growth rates of the strains were determined using a previously published
1107 MATLAB package[18].
1108
1109 **Streptomycin *Salmonella* Typhimurium Infection Model**
1110 Conventional mice were fasted for 4 hours before being treated with 100 µL of 200 mg/mL
1111 streptomycin (Sigma-Aldrich, S6501-50G) by oral gavage[30]. 24 hours later, mice were fasted for
1112 3 hours and infected by oral gavage with 100 µL of 10^6 CFU *Salmonella* Typhimurium. Fecal
1113 samples were collected daily for 3 days after *Salmonella* Typhimurium infection and spot-plated
1114 on streptomycin-LB agar plates.
1115
1116 **Bowel Preparation *Salmonella* Typhimurium Infection Model**
1117 Conventional mice underwent bowel prep as described previously and received oral gavage with
1118 100 µL of 10^6 CFU of wildtype *Salmonella* Typhimurium or *Salmonella* Typhimurium *ΔflhD* 6
1119 hours after the bowel prep. To assess dose-dependent *Salmonella* Typhimurium colonization, mice
1120 were infected with 10^2, 10^3, 10^5, 10^6, and 10^9 CFU post-bowel prep. To explore the susceptibility
1121 to *Salmonella* Typhimurium infection following bowel prep over time, mice were infected with
1122 10^6 CFU of *Salmonella* Typhimurium 6, 24, and 48 hours post-bowel prep. Fecal samples were
1123 collected daily for 3 days after *Salmonella* Typhimurium infection and spot-plated on Columbia
1124 Blood agar plates (per liter: 35 g Columbia Broth, 5% Sheep Blood, hemin, and vitamin K) to
1125 determine total absolute bacterial abundance and streptomycin-LB agar plates to determine
1126 absolute abundance of *Salmonella* Typhimurium.
1127
1128 **RNA extraction, Sequencing and Analysis**
1129 RNA was extracted from cecal tip tissue using the RNeasy Mini Kit (Qiagen) according to the
1130 manufacturer's instructions. The extracted RNA was sent to the Sequencing and Bioinformatics
1131 Consortium at UBC, where a sequencing library was prepared using a standard Illumina Stranded
1132 mRNA kit (Illumina) to generate 150 bp pair-end reads. Raw reads were assessed for nucleotide
1133 quality (terminal bases below PHRED quality score 20 were removed), trimmed to remove adaptor
1134 sequences, and merged using Fastp v. 0.23.4[98]. The reads were then aligned to the mouse genome
1135 GRCm39 using the STAR 2.7 software[99] with --quantMode GeneCounts, and the gene counts
1136 obtained were imported into R for downstream analyses. Raw gene counts were analysed using
1137 DESeq2[100]. For volcano plots, genes with adjusted p-value (Benjamin-Hochberg corrected) less
1138 than 0.05 and Log_2 fold change greater than 1.5 were highlighted. For select genes of interest, the

1139 Z-scores of the variance stabilized counts calculated using DESeq2 were plotted for all timepoints.
1140 Data visualization was performed using the tidyverse[92], pheatmap[101], and ggplot2[93] packages in R.
1141
1142 **Mammalian Cell Culture**
1143 Caco-2 and HT-29 cells were cultured individually in Dulbecco's Modified Eagle Medium
1144 (DMEM) high glucose (Sigma-Aldrich) supplemented with 10% (v/v) heat-inactivated fetal
1145 bovine serum (FBS, Corning), 1% (v/v) Penicillin-Streptomycin (Sigma-Aldrich), 1% (v/v)
1146 GlutaMAX supplement (Thermo Fisher), and 1% (v/v) non-essential amino acid (NEAA, Sigma-
1147 Aldrich) solution in T75 flasks (Corning). Cells were grown in humidified incubators at 37ºC
1148 and 5% CO_2. Media was replaced every other day and cells were passaged once they reached 60-
1149 70% confluency using 3 mL of TrypLE (Thermo Fisher) in a 1:10 split ratio.
1150
1151 Human Intestinal Microvascular Endothelial Cells (HIMECs) were cultured with complete
1152 endothelial cell growth medium (Sigma-Aldrich) and 1% (v/v) Penicillin-Streptomycin (Sigma-
1153 Aldrich) in humidified incubators at 37ºC and 5% CO_2. Frozen cells at passage 7 were thawed a
1154 week before experiment and seeded into a T75 flask (Corning) coated with 5 mL of Attachment
1155 Factor (Cell Systems). Media was changed every other day and cells were passaged once at 80%
1156 confluency using 3 mL of TrypLE by seeding 1 x 10^5 cells into an Attachment Factor-coated T75
1157 flask.
1158
1159 **Gut-on-a-Chip Culture**
1160 S1 chips (Emulate) were surface activated according to the manufacturer's protocol. Chips were
1161 then coated overnight in humidified incubators at 37ºC and 5% CO_2 with 200 µg/mL Collagen
1162 IV (Sigma-Aldrich) and 100 µg/mL Matrigel (Corning) in the apical channel, and 200 µg/mL
1163 Collagen IV and 30 µg/mL Fibronectin (Corning) in the basolateral channel, prepared in sterile
1164 cell-culture grade water. The following day, HIMECs at passage 8 were detached with TrypLE
1165 then resuspended to 8 x 10^6 cells/mL and 15 µL was seeded to the basolateral channel. Chips
1166 were flipped upside down and incubated for 1 hour to allow HIMECs to adhere. After flipping
1167 chips back, 4 parts of Caco-2 at passage 17 and 1 part of HT-29 at passage 16 detached with
1168 TrypLE were combined and resuspended to 7.5 x 10^6 cells/mL, and 35 µL was seeded to the
1169 apical channel. Cells were allowed to adhere overnight in the incubator, before connecting chips
1170 to continuous flow (60 µL/h) and mechanical deformation (10%, 0.15 Hz) and grown for 3
1171 additional days before switching to antibiotic-free DMEM high glucose with supplements in both
1172 channels.
1173
1174 **Chip Bowel Preparation and *Salmonella* Typhimurium Translocation Model**
1175 Bowel prep solution was prepared by dissolving 0.05 M polyethylene glycol (PEG)
1176 (commercially branded Restoralax) in DMEM high glucose or Hanks' Balanced Salt Solution
1177 (HBSS, Thermo Fisher). After 2 days of culture in antibiotic-free media, chips were treated with
1178 DMEM high glucose (~350 mOsm/kg) or bowel prep solution made with DMEM high glucose
1179 (~630 mOsm/kg) for 30 min at a 600 µL/h flow rate. Chips were disconnected from flow, and
1180 channel inlets and outlets were plugged with 200 µL filter tips as 50 µL of 10^6 CFU/mL
1181 *Salmonella* Typhimurium was seeded into the apical channel in HBSS or bowel prep solution
1182 made in HBSS, depending on the condition. Bacteria infected statically for 1 hour before filter
1183 tips were removed and chips were connected back to flow (120 µL/h) and mechanical

1184 deformation (10%, 0.15 Hz) in the incubator, with antibiotic-free DMEM high glucose with
1185 supplements. Media from all channels was sampled and spot-plated on LB-streptomycin agar
1186 plates at 4 hours and 24 hours post infection. After 24 hours, chips were disconnected then all
1187 channels were washed thrice with PBS (Gibco), fixed in 4% paraformaldehyde (Electron
1188 Microscopy Sciences) diluted with DPBS (Gibco).
1189
1190 **Paracellular Permeability Analysis**
1191 To assess paracellular permeability, 50 µg/ml of 3-5 kDa Fluorescein isothiocyanate-dextran
1192 (FITC-dextran, Sigma-Aldrich) was added to the apical channel media on the day before
1193 *Salmonella* Typhimurium infection. Chips were run under a 600 µL/h flow rate for 5 min to flush
1194 out existing media, then run at a 100 µL/h flow rate for 3 hours before samples from all channels
1195 were collected. Media was sampled prior to *Salmonella* Typhimurium infection to establish
1196 levels at baseline, after 4 hours of infection, and after 24 hours. The fluorescence intensities (490
1197 nm/520 nm) of the top and bottom channel effluents were measured using a Synergy H1 plate
1198 reader (Biotek) and FITC-dextran concentration was estimated by plotting a log-log standard
1199 curve. The apical to basolateral flux of FITC-dextran was calculated according to the following
1200 equation using the Emulate Apparent Permeability Calculator EC004v1.0[79]:
1201

1202 $$P_{app} = -\frac{Q_R * Q_D}{SA * (Q_R + Q_D)} * ln\left[1 - \frac{C_{R,0} * (Q_R + Q_D)}{(Q_R * C_{R,O} + Q_D * C_{D,0})}\right]$$

1203
1204 where P_{app} is the apparent permeability (cm/s); *SA* is the surface area of the sections of the
1205 channels that overlap (0.17 cm^2); Q_R and Q_D are the fluid flow rates in dosing and receiving
1206 channels, respectively (cm^3/s); and $C_{R,0}$ & $C_{D,0}$ are the recovered concentrations in the dosing
1207 and receiving channels, respectively.

1208
1209 **Quantification of Bacterial Colonization in Extraintestinal Tissues**
1210 Liver, mesenteric lymph nodes, and spleen were collected in pre-weighed sterile tubes filled with
1211 150 µL of PBS and weighed for final tissue mass. Tissues were homogenized at 300 Hz for 6
1212 minutes using the TissueLyser II (QIAGEN). Homogenized samples were serially diluted at 1:10
1213 in PBS, and all dilutions were spot-plated on both LB-streptomycin agar plates and Columbia
1214 Blood agar plates. Plates were incubated aerobically overnight at 37ºC. Single colonies were
1215 counted and back calculated to determine the absolute abundance of aerobic bacterial translocation
1216 to extraintestinal organs (mLN, spleen, and liver). Excess homogenized tissue was frozen at -80ºC
1217 for downstream 16S rRNA sequencing.
1218
1219 **Pathobiont Growth Measurements**
1220 1 µL of glycerol stocks of each of the 130 pathobionts isolated from UC patients were streaked on
1221 LB agar plates. A single colony was inoculated into 5 mL of liquid LB-streptomycin broth and
1222 grown for 17 hours overnight aerobically and shaking at 200 rpm. All strains were subcultured
1223 1:15 into LB broth in 2 mL 96 well plates, using a pipetting robot (INTEGRA VIAFLO384) and
1224 grown for 2 hours at 37ºC[18]. Strains were then inoculated at a ratio of 1:75 into LB media with pH
1225 levels of 4.0, 5.5, 6.9, and 8.0, and osmolality levels of 400, 800, 1200, and 1800 mOsm/Kg,
1226 adjusted with PEG. The experiments were conducted in technical triplicates using a 384-well plate.

1227
1228 Pathobiont bacterial growth curves were obtained using a Biotek Synergy H1 plate reader at 37°C
1229 for 24 hours either inside an anaerobic chamber (Coy Laboratories) with an atmosphere of 5%
1230 CO_2, 5% H_2, and 90% N2 (Linde Canada) or in aerobic conditions in parallel. The plates were
1231 shaken orbitally every 15 minutes following the collection of OD600 measurements. Background
1232 absorbance subtraction was performed from non-inoculated wells. The growth rates of the strains
1233 were determined using a previously published MATLAB package[18].
1234
1235 **Human Samples**
1236 All studies were approved by the Stanford University Institutional Review Board (IRB). Fecal
1237 samples were collected from patients with confirmed ulcerative colitis (UC) and from healthy
1238 controls. Stool samples were collected by patients at home in BIOME-Preserve tubes according to
1239 manufacturer instructions and returned to the research team within 24 hours, then snap-frozen with
1240 dry ice and stored at -80ºC until use. The fecal inocula for gavage were prepared in an anaerobic
1241 chamber, where 5g of feces from stool samples was resuspended in 10 mL of sterile and pre-
1242 reduced PBS and centrifuged at 4000 RPM for 5 minutes.
1243
1244 ***In vitro* hIBD Microbiota Growth**
1245 2 g of human stool inocula were grown from the frozen fecal samples in 5 mL of MEGA
1246 medium[18,102] aerobically overnight and subcultured 1:200 in fresh medium at baseline or adjusted
1247 to 800 mOsm/Kg with PEG. 16S rRNA sequencing was performed as described above (DNA
1248 Extraction, Library Preparation, and 16S rRNA Sequencing).
1249
1250 **Mouse Humanized Microbiota**
1251 Swiss Webster and C57BL/6J germ-free mice were inoculated with 200 µl of prepped fecal
1252 samples from human donors at 6 weeks of age by oral gavage (UC, hIBD or healthy control,
1253 hCTRL, respectively). In all experiments, offspring of inoculated mice between 8-12 weeks of age
1254 were used to ensure that mice were born with their respective microbiota. Stool was sampled
1255 approximately daily for two weeks (hIBD). Mice were sacrificed either before bowel prep (0 h),
1256 or at 24 hours or 2 weeks post-bowel prep and tissues were collected. Tissue was homogenized
1257 and plated as described above (Quantification of Bacterial Colonization in Extraintestinal Tissues).
1258 16S rRNA sequencing from mesenteric lymph nodes was performed on pooled plated samples as
1259 described above (DNA Extraction, Library Preparation, and 16S rRNA Sequencing).
1260
1261 **Statistics in Figures**
1262 For plating experiments where no CFUs were detected, the values were plotted at ½ the limit of
1263 detection (LoD) in log scale.
1264 $p > 0.05$; ns (not significant, not shown), $p < 0.05$; *, $p < 0.01$; **, $p < 0.001$; ***, $p < 0.0001$;
1265 ****.
1266
1267

1268 **Key resources table**

REAGENT or RESOURCE	SOURCE	IDENTIFIER
Bacterial Strains		
Salmonella enterica serovar Typhimurium SL1344	Gift from Finlay lab	n/a
Biological samples		
Human fecal samples from patients with ulcerative colitis and healthy controls	Sinha Lab	n/a
Potential pathobiont Enterobacteriaceae from patients with IBD library	Surette Lab	n/a
Chemicals, peptides, and recombinant proteins		
Polyethylene Glycol 3350	RestoraLAX	n/a
Methanol (Certified ACS)	Fisher Chemical	A412P-4
Chloroform (Ethanol as Preservative/Certified ACS)	Fisher Chemical	C298-500
Acetic Acid, Glacial (Certified ACS)	Fisher Chemical	X3P-1GAL
DAPI	Sigma Aldrich	D9542-5MG
WGA	Vector Laboratories	RL-1022
UEA-1	Vector Laboratories	FL-1061
Hematoxylin Solution, Gill No. 2	Sigma Aldrich	GHS216
Hydrochloric Acid Concentrate, 10N ACS (Certified)	Fisher Chemical	SA49
Ethyl Alcohol Anhydrous, USP	Greenfield Global	P016EAAN
Sodium Bicarbonate (Fine White Powder)	Fisher BioReagents	BP328-500
Magnesium Sulfate Heptahydrate	Fisher BioReagents	BP213-1
Eosin Y Solution, Alcoholic	Sigma Aldrich	HT110116
Permount™ Mounting Medium	Fisher Chemical	SP15-100

Phosphoric Acid, Certified, 25.0% (v/v) ±0.5% (v/v)	LabChem	LC186551
LB Broth, Miller	Fisher BioReagents	BP1426-500
Streptomycin sulfate salt	Sigma Aldrich	S6501-50G
Columbia Broth	BD DIFCO	294420
Sheep Blood (Defibrinated)	Dalynn Biologicals	HS30-500
Hemin Chloride	MilliporeSigma	37415GM
Vitamin K{1}	Thermo Scientific Chemicals	AAL1057506
DMEM, high glucose	Sigma-Aldrich	D6429
Fetal Bovine Serum, Regular	Corning	35-077-CV
Penicillin-Streptomycin	Sigma-Aldrich	P4333
GlutaMAX™ Supplement	Thermo Fisher	35050061
TrypLE	Thermo Fisher	12605010
Non-essential Amino Acid Solution	Sigma-Aldrich	M7145
Collagen IV	Sigma-Aldrich	C5533
Fibronectin	Corning	CLS356008
Corning™ Matrigel™ Matrix	Corning	CB-40234
Endothelial Cell Growth Medium MV 2	Sigma-Aldrich	C-22121
Attachment Factor	Cell Systems	4Z0-210
HBSS, calcium, magnesium	Thermo Fisher	14025092
Fluorescein isothiocyanate-dextran	Sigma-Aldrich	FD4
DPBS, no calcium, no magnesium	Gibco	14190144
Critical commercial assays		
S1 Chip	Emulate	n/a
Experimental models: Cell lines		

Caco-2 Cells	ATCC	HTB-37
HT-29 Cells	ATCC	HTB-38
Human Intestinal Microvascular Endothelial Cells	Cell Systems	ACBRI 666
Experimental models: Organisms/strains		
Mouse: C57BL/6J	Tropini Lab (originally Jackson Laboratories)	n/a
Mouse: Swiss Webster	Tropini Lab (originally Taconic)	n/a
Oligonucleotides		
16S V4 region 515F/926R primers (Forward primer: GTGYCAGCMGCCGCGGTAA-3', Reverse primer: CCGYCAATTYMTTTRAGTTT-3')	IDT	n/a
16S V4 region 515F/806R barcoded primers (Forward primer: GTGYCAGCMGCCGCGGTAA, Reverse primer: GGACTACNVGGGTWTCTAAT)	IDT	n/a
Software and algorithms		
QIIME2 (version 2023.9)	Bolyen et al. 2019[86]	
DADA2	Callahan et al. 2016[87]	
BacSpace	Earle et al. 2015[82]	
Fastp (version 0.23.4)	Chen et al. 2017[98]	
STAR 2.7	Dobin et al. 2013[99]	
Tidyverse (version 2.0.0)	Wickham et al. 2019[92]	
ggplot2 (version 3.5.1)	Hadley. 2016[93]	
Pheatmap (version 1.0.12)	https://rdrr.io/cran/pheatmap/	

1269

References

1. Seeff, L. C., Richards, T. B., Shapiro, J. A., Nadel, M. R., Manninen, D. L., Given, L. S., Dong, F. B., Winges, L. D. & McKenna, M. T. How many endoscopies are performed for colorectal cancer screening? Results from CDC's survey of endoscopic capacity. *Gastroenterology* **127,** 1670–1677 (2004).
2. Fukuyama, J., Rumker, L., Sankaran, K., Jeganathan, P., Dethlefsen, L., Relman, D. A. & Holmes, S. P. Multidomain analyses of a longitudinal human microbiome intestinal cleanout perturbation experiment. *PLoS Comput. Biol.* **13,** e1005706 (2017).
3. Nagata, N., Tohya, M., Fukuda, S., Suda, W., Nishijima, S., Takeuchi, F., Ohsugi, M., Tsujimoto, T., Nakamura, T., Shimomura, A., Yanagisawa, N., Hisada, Y., Watanabe, K., Imbe, K., Akiyama, J., Mizokami, M., Miyoshi-Akiyama, T., Uemura, N. & Hattori, M. Effects of bowel preparation on the human gut microbiome and metabolome. *Sci. Rep.* **9,** (2019).
4. Wang, P., Xu, T., Ngamruengphong, S., Makary, M. A., Kalloo, A. & Hutfless, S. Rates of infection after colonoscopy and osophagogastroduodenoscopy in ambulatory surgery centres in the USA. *Gut* **67,** 1626–1636 (2018).
5. Lin, J.-N., Wang, C.-B., Yang, C.-H., Lai, C.-H. & Lin, H.-H. Risk of infection following colonoscopy and sigmoidoscopy in symptomatic patients. *Endoscopy* **49,** 754–764 (2017).
6. Buret, A. G., Motta, J.-P., Allain, T., Ferraz, J. & Wallace, J. L. Pathobiont release from dysbiotic gut microbiota biofilms in intestinal inflammatory diseases: a role for iron? *J. Biomed. Sci.* **26,** 1 (2019).
7. Gomes-Neto, J. C., Kittana, H., Mantz, S., Segura Munoz, R. R., Schmaltz, R. J., Bindels, L. B., Clarke, J., Hostetter, J. M., Benson, A. K., Walter, J. & Ramer-Tait, A. E. A gut pathobiont synergizes with the microbiota to instigate inflammatory disease marked by immunoreactivity against other symbionts but not itself. *Sci. Rep.* **7,** 17707 (2017).
8. Bacsur, P., Rutka, M., Asbóth, A., Resál, T., Szántó, K., Jójárt, B., Bálint, A., Ari, E., Ajibola, W., Kintses, B., Fehér, T., Pigniczki, D., Bor, R., Fábián, A., Maléth, J., Szepes, Z., Farkas, K. & Molnár, T. Effects of bowel cleansing on the composition of the gut microbiota in inflammatory bowel disease patients and healthy controls. *Ther. Adv. Gastroenterol.* **16,** 17562848231174298 (2023).
9. Shobar, R. M., Velineni, S., Keshavarzian, A., Swanson, G., DeMeo, M. T., Melson, J. E., Losurdo, J., Engen, P. A., Sun, Y., Koenig, L. & Mutlu, E. A. The Effects of Bowel Preparation on Microbiota-Related Metrics Differ in Health and in Inflammatory Bowel Disease and for the Mucosal and Luminal Microbiota Compartments. *Clin. Transl. Gastroenterol.* **7,** e143 (2016).
10. Schwesinger, W. H., Levine, B. A. & Ramos, R. Complications in colonoscopy. *Surg. Gynecol. Obstet.* **148,** 270–281 (1979).
11. Kim, E. S., Kim, K. O., Jang, B. I., Kim, E. Y., Lee, Y. J., Lee, H. S., Jeon, S. W., Kim, H. J. & Kim, S. K. Comparison of 4-L Polyethylene Glycol and 2-L Polyethylene Glycol Plus Ascorbic Acid in Patients with Inactive Ulcerative Colitis. *Dig. Dis. Sci.* **62,** 2489–2497 (2017).
12. Menees, S., Higgins, P., Korsnes, S. & Elta, G. Does colonoscopy cause increased ulcerative colitis symptoms? *Inflamm. Bowel Dis.* **13,** 12–18 (2007).

1313 13. Tariq, S., Farooq, A., Ali, I. & Wijesinghe, H. Toxic colonoscopy-how investigating active
1314 inflammatory bowel disease can lead to the serious complication of toxic megacolon.
1315 (2015). doi:10.1136/bcr-2015
1316 14. Burnett-Hartman, A. N., Hua, X., Rue, T. C., Golchin, N., Kessler, L. & Rowhani-Rahbar,
1317 A. Risk interval analysis of emergency room visits following colonoscopy in patients with
1318 inflammatory bowel disease. *PLoS ONE* **14,** (2019).
1319 15. Peiqi, W., Saowanee, N., Florin, S., Alyssa, P., Joanna, M., Mark, L. & Susan, H. Young
1320 Investigator: Complications After Colonoscopy in Patients With Inflammatory Bowel
1321 Disease: P-016. *Off. J. Am. Coll. Gastroenterol. ACG* **113,** (2018).
1322 16. Goetz, M. Endoscopic Surveillance in Inflammatory Bowel Disease. *Visc. Med.* **34,** 66–71
1323 (2018).
1324 17. Tropini, C., Moss, E. L., Merrill, B. D., Ng, K. M., Higginbottom, S. K., Casavant, E. P.,
1325 Gonzalez, C. G., Fremin, B., Bouley, D. M., Elias, J. E., Bhatt, A. S., Huang, K. C. &
1326 Sonnenburg, J. L. Transient Osmotic Perturbation Causes Long-Term Alteration to the Gut
1327 Microbiota. *Cell* **173,** 1742—1754.e17 (2018).
1328 18. Ng, K. M., Pannu, S., Liu, S., Burckhardt, J. C., Hughes, T., Van Treuren, W., Nguyen, J.,
1329 Naqvi, K., Nguyen, B., Clayton, C. A., Pepin, D. M., Collins, S. R. & Tropini, C. Single-
1330 strain behavior predicts responses to environmental pH and osmolality in the gut
1331 microbiota. *mBio* **14,** e00753-23 (2023).
1332 19. Ferreyra, J. A., Wu, K. J., Hryckowian, A. J., Bouley, D. M., Weimer, B. C. & Sonnenburg,
1333 J. L. Gut microbiota-produced succinate promotes C. Difficile infection after antibiotic
1334 treatment or motility disturbance. *Cell Host Microbe* **16,** 770–777 (2014).
1335 20. Schuchat, A., Deaver, K. A., Wenger, J. D., Plikaytis, B. D., Mascola, L., Pinner, R. W.,
1336 Reingold, A. L. & Broome, C. V. Role of foods in sporadic listeriosis. I. Case-control study
1337 of dietary risk factors. The Listeria Study Group. *JAMA* **267,** 2041–2045 (1992).
1338 21. Tomkovich, S., Taylor, A., King, J., Colovas, J., Bishop, L., McBride, K., Royzenblat, S.,
1339 Lesniak, N. A., Bergin, I. L. & Schloss, P. D. An Osmotic Laxative Renders Mice
1340 Susceptible to Prolonged Clostridioides difficile Colonization and Hinders Clearance.
1341 *mSphere* **6,** (2021).
1342 22. Que, J. U. & Hentges, D. J. Effect of streptomycin administration on colonization resistance
1343 to Salmonella typhimurium in mice. *Infect. Immun.* **48,** 169–174 (1985).
1344 23. Lawley, T. D., Bouley, D. M., Hoy, Y. E., Gerke, C., Relman, D. A. & Monack, D. M. Host
1345 Transmission of Salmonella enterica Serovar Typhimurium Is Controlled by Virulence
1346 Factors and Indigenous Intestinal Microbiota. *Infect. Immun.* **76,** 403–416 (2008).
1347 24. Tropini, C., Earle, K. A., Huang, K. C. & Sonnenburg, J. L. The Gut Microbiome:
1348 Connecting Spatial Organization to Function. *Cell Host Microbe* **21,** 433–442 (2017).
1349 25. McCallum, G. & Tropini, C. The gut microbiota and its biogeography. *Nat. Rev. Microbiol.*
1350 **22,** 105–118 (2024).
1351 26. David, L. A., Weil, A., Ryan, E. T., Calderwood, S. B., Harris, J. B., Chowdhury, F., Begum,
1352 Y., Qadri, F., LaRocque, R. C. & Turnbaugh, P. J. Gut Microbial Succession Follows Acute
1353 Secretory Diarrhea in Humans. *mBio* **6,** e00381--15 (2015).
1354 27. Sun, Y. & O'Riordan, M. X. D. Regulation of Bacterial Pathogenesis by Intestinal Short-
1355 Chain Fatty Acids. *Adv. Appl. Microbiol.* **85,** 93–118 (2013).
1356 28. Desai, M. S., Seekatz, A. M., Koropatkin, N. M., Kamada, N., Hickey, C. A., Wolter, M.,
1357 Pudlo, N. A., Kitamoto, S., Terrapon, N., Muller, A., Young, V. B., Henrissat, B., Wilmes,

1358 P., Stappenbeck, T. S., Núñez, G. & Martens, E. C. A Dietary Fiber-Deprived Gut
1359 Microbiota Degrades the Colonic Mucus Barrier and Enhances Pathogen Susceptibility.
1360 *Cell* **167,** 1339-1353.e21 (2016).
1361 29. Csonka, L. N. Physiological and genetic responses of bacteria to osmotic stress. *Microbiol.*
1362 *Rev.* **53,** 121–147 (1989).
1363 30. Barthel, M., Hapfelmeier, S., Quintanilla-Martínez, L., Kremer, M., Rohde, M., Hogardt, M.,
1364 Pfeffer, K., Rüssmann, H. & Hardt, W. D. Pretreatment of mice with streptomycin provides
1365 a Salmonella enterica serovar Typhimurium colitis model that allows analysis of both
1366 pathogen and host. *Infect. Immun.* **71,** 2839–2858 (2003).
1367 31. Furter, M., Sellin, M. E., Hansson, G. C. & Hardt, W. D. Mucus Architecture and Near-
1368 Surface Swimming Affect Distinct Salmonella Typhimurium Infection Patterns along the
1369 Murine Intestinal Tract. *Cell Rep.* **27,** 2665-2678.e3 (2019).
1370 32. Hallstrom, K. & McCormick, B. A. Salmonella Interaction with and Passage through the
1371 Intestinal Mucosa: Through the Lens of the Organism. *Front. Microbiol.* **2,** (2011).
1372 33. Terashima, H., Kojima, S. & Homma, M. in *Int. Rev. Cell Mol. Biol.* **270,** 39–85 (Academic
1373 Press, 2008).
1374 34. Hoffmann, P., Burmester, M., Langeheine, M., Brehm, R., Empl, M. T., Seeger, B. &
1375 Breves, G. Caco-2/HT29-MTX co-cultured cells as a model for studying physiological
1376 properties and toxin-induced effects on intestinal cells. *PLOS ONE* **16,** e0257824 (2021).
1377 35. Ahmad, R., Sorrell, M. F., Batra, S. K., Dhawan, P. & Singh, A. B. Gut permeability and
1378 mucosal inflammation: bad, good or context dependent. *Mucosal Immunol.* **10,** 307–317
1379 (2017).
1380 36. Enriquez, J., Mims, B. M. D., Trasti, S., Furr, K. L. & Grisham, M. B. Genomic, microbial
1381 and environmental standardization in animal experimentation limiting immunological
1382 discovery. *BMC Immunol.* **21,** 50 (2020).
1383 37. Walker, G. T., Gerner, R. R., Nuccio, S.-P. & Raffatellu, M. Murine Models of Salmonella
1384 Infection. *Curr. Protoc.* **3,** e824 (2023).
1385 38. Stecher, B., Hapfelmeier, S., Müller, C., Kremer, M., Stallmach, T. & Hardt, W.-D. Flagella
1386 and Chemotaxis Are Required for Efficient Induction of Salmonella enterica Serovar
1387 Typhimurium Colitis in Streptomycin-Pretreated Mice. *Infect. Immun.* **72,** 4138–4150
1388 (2004).
1389 39. Gantois, I., Ducatelle, R., Pasmans, F., Haesebrouck, F., Hautefort, I., Thompson, A.,
1390 Hinton, J. C. & Van Immerseel, F. Butyrate Specifically Down-Regulates Salmonella
1391 Pathogenicity Island 1 Gene Expression. *Appl. Environ. Microbiol.* **72,** 946–949 (2006).
1392 40. Anderson, C. J. & Kendall, M. M. Salmonella enterica Serovar Typhimurium Strategies for
1393 Host Adaptation. *Front. Microbiol.* **8,** (2017).
1394 41. Johansson, M. E. V., Gustafsson, J. K., Holmén-Larsson, J., Jabbar, K. S., Xia, L., Xu, H.,
1395 Ghishan, F. K., Carvalho, F. A., Gewirtz, A. T., Sjövall, H. & Hansson, G. C. Bacteria
1396 penetrate the normally impenetrable inner colon mucus layer in both murine colitis models
1397 and patients with ulcerative colitis. *Gut* **63,** 281–291 (2013).
1398 42. Bergstrom, K. S. B., Kissoon-Singh, V., Gibson, D. L., Ma, C., Montero, M., Sham, H. P.,
1399 Ryz, N., Huang, T., Velcich, A., Finlay, B. B., Chadee, K. & Vallance, B. A. Muc2 protects
1400 against lethal infectious colitis by disassociating pathogenic and commensal bacteria from
1401 the colonic mucosa. *PLoS Pathog.* **6,** (2010).

1402 43. Zarepour, M., Bhullar, K., Montero, M., Ma, C., Huang, T., Velcich, A., Xia, L. & Vallance,
1403 B. A. The Mucin Muc2 Limits Pathogen Burdens and Epithelial Barrier Dysfunction during
1404 Salmonella enterica Serovar Typhimurium Colitis. *Infect. Immun.* **81,** 3672–3683 (2013).
1405 44. Xu, H., Feng, Y., Du, Y., Han, Y., Duan, X., Jiang, Y., Su, L., Liu, X., Qin, S., He, K. &
1406 Huang, J. Bacterial–host adhesion dominated by collagen subtypes remodelled by osmotic
1407 pressure. *Npj Biofilms Microbiomes* **10,** 1–12 (2024).
1408 45. Ng, K. M., Aranda-Díaz, A., Tropini, C., Frankel, M. R., Van Treuren, W., O'Laughlin, C.
1409 T., Merrill, B. D., Yu, F. B., Pruss, K. M., Oliveira, R. A., Higginbottom, S. K., Neff, N. F.,
1410 Fischbach, M. A., Xavier, K. B., Sonnenburg, J. L. & Huang, K. C. Recovery of the Gut
1411 Microbiota after Antibiotics Depends on Host Diet, Community Context, and
1412 Environmental Reservoirs. *Cell Host Microbe* **26,** 650-665.e4 (2019).
1413 46. Stecher, B., Barthel, M., Schlumberger, M. C., Haberli, L., Rabsch, W., Kremer, M. & Hardt,
1414 W.-D. Motility allows S. Typhimurium to benefit from the mucosal defence. *Cell.*
1415 *Microbiol.* **10,** 1166–1180 (2008).
1416 47. Modification of Salmonella Typhimurium Motility by the Probiotic Yeast Strain
1417 Saccharomyces boulardii | PLOS ONE. at
1418 <https://journals.plos.org/plosone/article?id=10.1371/journal.pone.0033796>
1419 48. Compound(s) secreted by Lactobacilluscasei strain Shirota YIT9029 irreversibly and
1420 reversibly impair the swimming motility of Helicobacter pylori and Salmonella enterica
1421 serovar Typhimurium, respectively | Microbiology Society. at
1422 <https://www.microbiologyresearch.org/content/journal/micro/10.1099/mic.0.067678-
1423 0#tab2>
1424 49. Li, B., Yue, Y., Yuan, Z., Zhang, F., Li, P., Song, N., Lin, W., Liu, Y., Yang, Y., Li, Z. &
1425 Gu, L. Salmonella STM1697 coordinates flagella biogenesis and virulence by restricting
1426 flagellar master protein FlhD4C2 from recruiting RNA polymerase. *Nucleic Acids Res.* **45,**
1427 9976–9989 (2017).
1428 50. Das, C., Mokashi, C., Mande, S. S. & Saini, S. Dynamics and Control of Flagella Assembly
1429 in Salmonella typhimurium. *Front. Cell. Infect. Microbiol.* **8,** (2018).
1430 51. Karlinsey, J. E., Lonner, J., Brown, K. L. & Hughes, K. T. Translation/Secretion Coupling
1431 by Type III Secretion Systems. *Cell* **102,** 487–497 (2000).
1432 52. Fàbrega, A. & Vila, J. Salmonella enterica serovar Typhimurium skills to succeed in the
1433 host: virulence and regulation. *Clin. Microbiol. Rev.* **26,** 308–341 (2013).
1434 53. Liu, X., Lu, R., Xia, Y. & Sun, J. Global analysis of the eukaryotic pathways and networks
1435 regulated by Salmonella typhimurium in mouse intestinal infection in vivo. *BMC Genomics*
1436 **11,** 722 (2010).
1437 54. Hoogerwerf, W. A., Sinha, M., Conesa, A., Luxon, B. A., Shahinian, V. B., Cornélissen, G.,
1438 Halberg, F., Bostwick, J., Timm, J. & Cassone, V. M. Transcriptional profiling of mRNA
1439 expression in the mouse distal colon. *Gastroenterology* **135,** 2019–2029 (2008).
1440 55. Parnaud, G., Corpet, D. E. & Gamet-Payrastre, L. Cytostatic effect of polyethylene glycol on
1441 human colonic adenocarcinoma cells. *Int. J. Cancer* **92,** 63–69 (2001).
1442 56. Gazzaniga, F. S., Camacho, D. M., Wu, M., Silva Palazzo, M. F., Dinis, A. L. M., Grafton,
1443 F. N., Cartwright, M. J., Super, M., Kasper, D. L. & Ingber, D. E. Harnessing Colon Chip
1444 Technology to Identify Commensal Bacteria That Promote Host Tolerance to Infection.
1445 *Front. Cell. Infect. Microbiol.* **11,** (2021).

1446 57. Lloyd-Price, J., Arze, C., Ananthakrishnan, A. N., Schirmer, M., Avila-Pacheco, J., Poon,
1447 tiffany W., Andrews, E., Ajami, N. J., Bonham, K. S., Brislawn, colin J., Casero, D.,
1448 Courtney, H., Gonzalez, A., Graeber, thomas G., Hall, A. B., Lake, K., Landers, carol J.,
1449 Mallick, H., Plichta, D. R., Prasad, M., Rahnavard, G., Sauk, J., Shungin, D., Vázquez-
1450 Baeza, Y., White, R. A., Bishai, J., Bullock, K., Deik, A., Dennis, C., Kaplan, J. L., Khalili,
1451 H., McIver, L. J., Moran, C. J., Nguyen, L., Pierce, K. A., Schwager, R., Sirota-Madi, A.,
1452 Stevens, B. W., Tan, W., ten Hoeve, J. J., Weingart, G., Wilson, R. G., Yajnik, V., Braun,
1453 J., Denson, L. A., Jansson, J. K., Knight, R., Kugathasan, S., McGovern, D. P. B.,
1454 Petrosino, J. F., Stappenbeck, T. S., Winter, H. S., Clish, clary B., Franzosa, eric A.,
1455 Vlamakis, H., Xavier, ramnik J. & Huttenhower, C. Multi-omics of the gut microbial
1456 ecosystem in inflammatory bowel diseases. *Nature* **569,** 655–662 (2019).
1457 58. Schirmer, M., Denson, L., Vlamakis, H., Franzosa, E. A., Thomas, S., Gotman, N. M., Rufo,
1458 P., Baker, S. S., Sauer, C., Markowitz, J., Pfefferkorn, M., Oliva-Hemker, M., Rosh, J.,
1459 Otley, A., Boyle, B., Mack, D., Baldassano, R., Keljo, D., LeLeiko, N., Heyman, M.,
1460 Griffiths, A., Patel, A. S., Noe, J., Kugathasan, S., Walters, T., Huttenhower, C., Hyams, J.
1461 & Xavier, R. J. Compositional and temporal changes in the gut microbiome of pediatric
1462 ulcerative colitis patients are linked to disease course. *Cell Host Microbe* **24,** 600-610.e4
1463 (2018).
1464 59. Gevers, D., Kugathasan, S., Denson, L. A., Vázquez-Baeza, Y., Van Treuren, W., Ren, B.,
1465 Schwager, E., Knights, D., Song, S. J., Yassour, M., Morgan, X. C., Kostic, A. D., Luo, C.,
1466 González, A., McDonald, D., Haberman, Y., Walters, T., Baker, S., Rosh, J., Stephens, M.,
1467 Heyman, M., Markowitz, J., Baldassano, R., Griffiths, A., Sylvester, F., Mack, D., Kim, S.,
1468 Crandall, W., Hyams, J., Huttenhower, C., Knight, R. & Xavier, R. J. The treatment-naïve
1469 microbiome in new-onset Crohn's disease. *Cell Host Microbe* **15,** 382–392 (2014).
1470 60. Jalili-Firoozinezhad, S., Prantil-Baun, R., Jiang, A., Potla, R., Mammoto, T., Weaver, J. C.,
1471 Ferrante, T. C., Kim, H. J., Cabral, J. M. S., Levy, O. & Ingber, D. E. Modeling radiation
1472 injury-induced cell death and countermeasure drug responses in a human Gut-on-a-Chip.
1473 *Cell Death Dis.* **9,** 1–14 (2018).
1474 61. Jalili-Firoozinezhad, S., Gazzaniga, F. S., Calamari, E. L., Camacho, D. M., Fadel, C. W.,
1475 Bein, A., Swenor, B., Nestor, B., Cronce, M. J., Tovaglieri, A., Levy, O., Gregory, K. E.,
1476 Breault, D. T., Cabral, J. M. S., Kasper, D. L., Novak, R. & Ingber, D. E. A complex human
1477 gut microbiome cultured in an anaerobic intestine-on-a-chip. *Nat. Biomed. Eng.* **3,** 520–531
1478 (2019).
1479 62. Bein, A., Fadel, C. W., Swenor, B., Cao, W., Powers, R. K., Camacho, D. M., Naziripour,
1480 A., Parsons, A., LoGrande, N., Sharma, S., Kim, S., Jalili-Firoozinezhad, S., Grant, J.,
1481 Breault, D. T., Iqbal, J., Ali, A., Denson, L. A., Moore, S. R., Prantil-Baun, R., Goyal, G. &
1482 Ingber, D. E. Nutritional deficiency in an intestine-on-a-chip recapitulates injury hallmarks
1483 associated with environmental enteric dysfunction. *Nat. Biomed. Eng.* **6,** 1236–1247 (2022).
1484 63. Takahashi, J. S. Transcriptional architecture of the mammalian circadian clock. *Nat. Rev.*
1485 *Genet.* **18,** 164–179 (2017).
1486 64. Ripperger, J. A., Jud, C. & Albrecht, U. The daily rhythm of mice. *FEBS Lett.* **585,** 1384–
1487 1392 (2011).
1488 65. Period2 3′-UTR and microRNA-24 regulate circadian rhythms by repressing PERIOD2
1489 protein accumulation | PNAS. at
1490 <https://www.pnas.org/doi/full/10.1073/pnas.1706611114>

1491 66. Voigt, R. M., Forsyth, C. B. & Keshavarzian, A. Circadian rhythms: a regulator of
1492 gastrointestinal health and dysfunction. *Expert Rev. Gastroenterol. Hepatol.* **13,** 411–424
1493 (2019).
1494 67. Sun, J., Liu, X., Gao, H., Zhang, L., Ji, Q., Wang, Z., Zhou, L., Wang, Y., Sui, H., Fan, Z. &
1495 Li, Q. Overexpression of colorectal cancer oncogene CHRDL2 predicts a poor prognosis.
1496 *Oncotarget* **8,** 11489–11506 (2016).
1497 68. Nayerpour Dizaj, T., Doustmihan, A., Sadeghzadeh Oskouei, B., Akbari, M., Jaymand, M.,
1498 Mazloomi, M. & Jahanban-Esfahlan, R. Significance of PSCA as a novel prognostic marker
1499 and therapeutic target for cancer. *Cancer Cell Int.* **24,** 135 (2024).
1500 69. Metzger, R., Winter, L., Bouznad, N., Garzetti, D., von Armansperg, B., Rokavec, M., Lutz,
1501 K., Schäfer, Y., Krebs, S., Winheim, E., Friedrich, V., Matzek, D., Öllinger, R., Rad, R.,
1502 Stecher, B., Hermeking, H., Brocker, T. & Krug, A. B. CCL17 Promotes Colitis-Associated
1503 Tumorigenesis Dependent on the Microbiota. *J. Immunol.* **209,** 2227–2238 (2022).
1504 70. Zhao, T., Li, Y., Shen, K., Wang, Q. & Zhang, J. Knockdown of OLR1 weakens glycolytic
1505 metabolism to repress colon cancer cell proliferation and chemoresistance by
1506 downregulating SULT2B1 via c-MYC. *Cell Death Dis.* **13,** 1–12 (2021).
1507 71. Grunnet, M., Jespersen, T., Rasmussen, H. B., Ljungstrøm, T., Jorgensen, N. K., Olesen, S.-
1508 P. & Klaerke, D. A. KCNE4 is an inhibitory subunit to the KCNQ1 channel. *J. Physiol.*
1509 **542,** 119–130 (2002).
1510 72. Crawford, R. R., Prescott, E. T., Sylvester, C. F., Higdon, A. N., Shan, J., Kilberg, M. S. &
1511 Mungrue, I. N. Human CHAC1 Protein Degrades Glutathione, and mRNA Induction Is
1512 Regulated by the Transcription Factors ATF4 and ATF3 and a Bipartite ATF/CRE
1513 Regulatory Element. *J. Biol. Chem.* **290,** 15878–15891 (2015).
1514 73. Xu, H., Ghishan, F. K. & Kiela, P. R. SLC9 Gene Family: Function, Expression, and
1515 Regulation. *Compr. Physiol.* **8,** 555–583 (2018).
1516 74. Courteau, L., Crasto, J., Hassanzadeh, G., Baird, S. D., Hodgins, J., Liwak-Muir, U., Fung,
1517 G., Luo, H., Stojdl, D. F., Screaton, R. A. & Holcik, M. Hexokinase 2 controls cellular
1518 stress response through localization of an RNA-binding protein. *Cell Death Dis.* **6,** e1837–
1519 e1837 (2015).
1520 75. Takebe, K., Nio, J., Morimatsu, M., Karaki, S.-I., Kuwahara, A., Kato, I. & Iwanaga, T.
1521 Histochemical demonstration of a Na+-coupled transporter for short-chain fatty acids
1522 (Slc5a8) in the intestine and kidney of the mouse. *Biomed. Res.* **26,** 213–221 (2005).
1523 76. Shashikanth, N., France, M. M., Xiao, R., Haest, X., Rizzo, H. E., Yeste, J., Reiner, J. &
1524 Turner, J. R. Tight junction channel regulation by interclaudin interference. *Nat. Commun.*
1525 **13,** 3780 (2022).
1526 77. Zheng, D., Kern, L. & Elinav, E. The NLRP6 inflammasome. *Immunology* **162,** 281–289
1527 (2021).
1528 78. Zhang, N., Heruth, D. P., Wu, W., Zhang, L. Q., Nsumu, M. N., Shortt, K., Li, K., Jiang, X.,
1529 Wang, B., Friesen, C., Li, D.-Y. & Ye, S. Q. Functional characterization of SLC26A3
1530 c.392C\textgreaterG (p.P131R) mutation in intestinal barrier function using
1531 CRISPR/CAS9-created cell models. *Cell Biosci.* **9,** 40 (2019).
1532 79. Barrier Function Readout Analysis. *Emulate* at <https://emulatebio.com/support/ep187-v1-
1533 0/>

1534 80. Wrzosek, L., Ciocan, D., Borentain, P., Spatz, M., Puchois, V., Hugot, C., Ferrere, G.,
1535 Mayeur, C., Perlemuter, G. & Cassard, A.-M. Transplantation of human microbiota into
1536 conventional mice durably reshapes the gut microbiota. *Sci. Rep.* **8,** 6854 (2018).
1537 81. Ng, K. M. & Tropini, C. Visualization of Gut Microbiota-host Interactions via Fluorescence
1538 In Situ Hybridization, Lectin Staining, and Imaging. *JoVE J. Vis. Exp.* e62646 (2021).
1539 doi:10.3791/62646
1540 82. Earle, K. A., Billings, G., Sigal, M., Lichtman, J. S., Hansson, G. C., Elias, J. E., Amieva, M.
1541 R., Huang, K. C. & Sonnenburg, J. L. Quantitative Imaging of Gut Microbiota Spatial
1542 Organization. *Cell Host Microbe* **18,** 478–488 (2015).
1543 83. An Intro to H&E Staining: Protocol, Best Practices, Steps & More. at
1544 <https://www.leicabiosystems.com/en-ca/knowledge-pathway/he-staining-overview-a-
1545 guide-to-best-practices/>
1546 84. De Wolfe, T. J. & Wright, E. S. Multi-factorial examination of amplicon sequencing
1547 workflows from sample preparation to bioinformatic analysis. *BMC Microbiol.* **23,** 107
1548 (2023).
1549 85. Andrews, S. FastQC: A Quality Control tool for High Throughput Sequence Data. *FASTQC*
1550 *Qual. Control Tool High Throughput Seq. Data* (2010). at
1551 <https://www.bioinformatics.babraham.ac.uk/projects/fastqc/>
1552 86. Bolyen, E., Rideout, J. R., Dillon, M. R., Bokulich, N. A., Abnet, C. C., Al-Ghalith, G. A.,
1553 Alexander, H., Alm, E. J., Arumugam, M., Asnicar, F., Bai, Y., Bisanz, J. E., Bittinger, K.,
1554 Brejnrod, A., Brislawn, C. J., Brown, C. T., Callahan, B. J., Caraballo-Rodríguez, A. M.,
1555 Chase, J., Cope, E. K., Da Silva, R., Diener, C., Dorrestein, P. C., Douglas, G. M., Durall,
1556 D. M., Duvallet, C., Edwardson, C. F., Ernst, M., Estaki, M., Fouquier, J., Gauglitz, J. M.,
1557 Gibbons, S. M., Gibson, D. L., Gonzalez, A., Gorlick, K., Guo, J., Hillmann, B., Holmes,
1558 S., Holste, H., Huttenhower, C., Huttley, G. A., Janssen, S., Jarmusch, A. K., Jiang, L.,
1559 Kaehler, B. D., Kang, K. B., Keefe, C. R., Keim, P., Kelley, S. T., Knights, D., Koester, I.,
1560 Kosciolek, T., Kreps, J., Langille, M. G. I., Lee, J., Ley, R., Liu, Y.-X., Loftfield, E.,
1561 Lozupone, C., Maher, M., Marotz, C., Martin, B. D., McDonald, D., McIver, L. J., Melnik,
1562 A. V., Metcalf, J. L., Morgan, S. C., Morton, J. T., Naimey, A. T., Navas-Molina, J. A.,
1563 Nothias, L. F., Orchanian, S. B., Pearson, T., Peoples, S. L., Petras, D., Preuss, M. L.,
1564 Pruesse, E., Rasmussen, L. B., Rivers, A., Robeson, M. S., Rosenthal, P., Segata, N.,
1565 Shaffer, M., Shiffer, A., Sinha, R., Song, S. J., Spear, J. R., Swafford, A. D., Thompson, L.
1566 R., Torres, P. J., Trinh, P., Tripathi, A., Turnbaugh, P. J., Ul-Hasan, S., van der Hooft, J. J.
1567 J., Vargas, F., Vázquez-Baeza, Y., Vogtmann, E., von Hippel, M., Walters, W., Wan, Y.,
1568 Wang, M., Warren, J., Weber, K. C., Williamson, C. H. D., Willis, A. D., Xu, Z. Z.,
1569 Zaneveld, J. R., Zhang, Y., Zhu, Q., Knight, R. & Caporaso, J. G. Reproducible, interactive,
1570 scalable and extensible microbiome data science using QIIME 2. *Nat. Biotechnol.* **37,** 852–
1571 857 (2019).
1572 87. Callahan, B. J., McMurdie, P. J., Rosen, M. J., Han, A. W., Johnson, A. J. A. & Holmes, S.
1573 P. DADA2: High-resolution sample inference from Illumina amplicon data. *Nat. Methods*
1574 **13,** 581–583 (2016).
1575 88. Quast, C., Pruesse, E., Yilmaz, P., Gerken, J., Schweer, T., Yarza, P., Peplies, J. & Glöckner,
1576 F. O. The SILVA ribosomal RNA gene database project: improved data processing and
1577 web-based tools. *Nucleic Acids Res.* **41,** D590–D596 (2013).

89. Katoh, K., Misawa, K., Kuma, K. & Miyata, T. MAFFT: a novel method for rapid multiple sequence alignment based on fast Fourier transform. *Nucleic Acids Res.* **30,** 3059–3066 (2002).
90. Price, M. N., Dehal, P. S. & Arkin, A. P. FastTree 2 – Approximately Maximum-Likelihood Trees for Large Alignments. *PLOS ONE* **5,** e9490 (2010).
91. team, R. C. R: A language and environment for statistical computing. (2021). at <https://www.r-project.org/>
92. Wickham, H., Averick, M., Bryan, J., Chang, W., McGowan, L. D., François, R., Grolemund, G., Hayes, A., Henry, L., Hester, J., Kuhn, M., Pedersen, T. L., Miller, E., Bache, S. M., Müller, K., Ooms, J., Robinson, D., Seidel, D. P., Spinu, V., Takahashi, K., Vaughan, D., Wilke, C., Woo, K. & Yutani, H. Welcome to the Tidyverse. *J. Open Source Softw.* **4,** 1686 (2019).
93. Hadley, W. *ggplot2: Elegant Graphics for Data Analysis*. (Springer-Verlag New York, 2016). at <https://ggplot2/tidyverse.org>
94. McMurdie, P. J. & Holmes, S. phyloseq: An R Package for Reproducible Interactive Analysis and Graphics of Microbiome Census Data. *PLOS ONE* **8,** e61217 (2013).
95. Kassambara, A. ggpubr: 'ggplot2' Based Publication Ready Plots. (2023). at <https://rpkgs.datanovia.com/ggpubr/>
96. Dixon, P. VEGAN, a package of R functions for community ecology. *J. Veg. Sci.* **14,** 927–930 (2003).
97. Li, J., Yang, K., Ju, T., Ho, T., McKay, C. A., Gao, Y., Forget, S. K., Gartner, S. R., Field, C. J., Chan, C. B. & Willing, B. P. Early life antibiotic exposure affects pancreatic islet development and metabolic regulation. *Sci. Rep.* **7,** 41778 (2017).
98. Chen, S., Zhou, Y., Chen, Y. & Gu, J. fastp: an ultra-fast all-in-one FASTQ preprocessor. *Bioinformatics* **34,** i884–i890 (2018).
99. Dobin, A., Davis, C. A., Schlesinger, F., Drenkow, J., Zaleski, C., Jha, S., Batut, P., Chaisson, M. & Gingeras, T. R. STAR: ultrafast universal RNA-seq aligner. *Bioinformatics* **29,** 15–21 (2013).
100. Love, M. I., Huber, W. & Anders, S. Moderated estimation of fold change and dispersion for RNA-seq data with DESeq2. *Genome Biol.* **15,** 550 (2014).
101. pheatmap: Pretty Heatmaps version 1.0.12 from CRAN. at <https://rdrr.io/cran/pheatmap/>
102. Han, S., Van Treuren, W., Fischer, C. R., Merrill, B. D., DeFelice, B. C., Sanchez, J. M., Higginbottom, S. K., Guthrie, L., Fall, L. A., Dodd, D., Fischbach, M. A. & Sonnenburg, J. L. A metabolomics pipeline for the mechanistic interrogation of the gut microbiome. *Nat. 2021 5957867* **595,** 415–420 (2021).

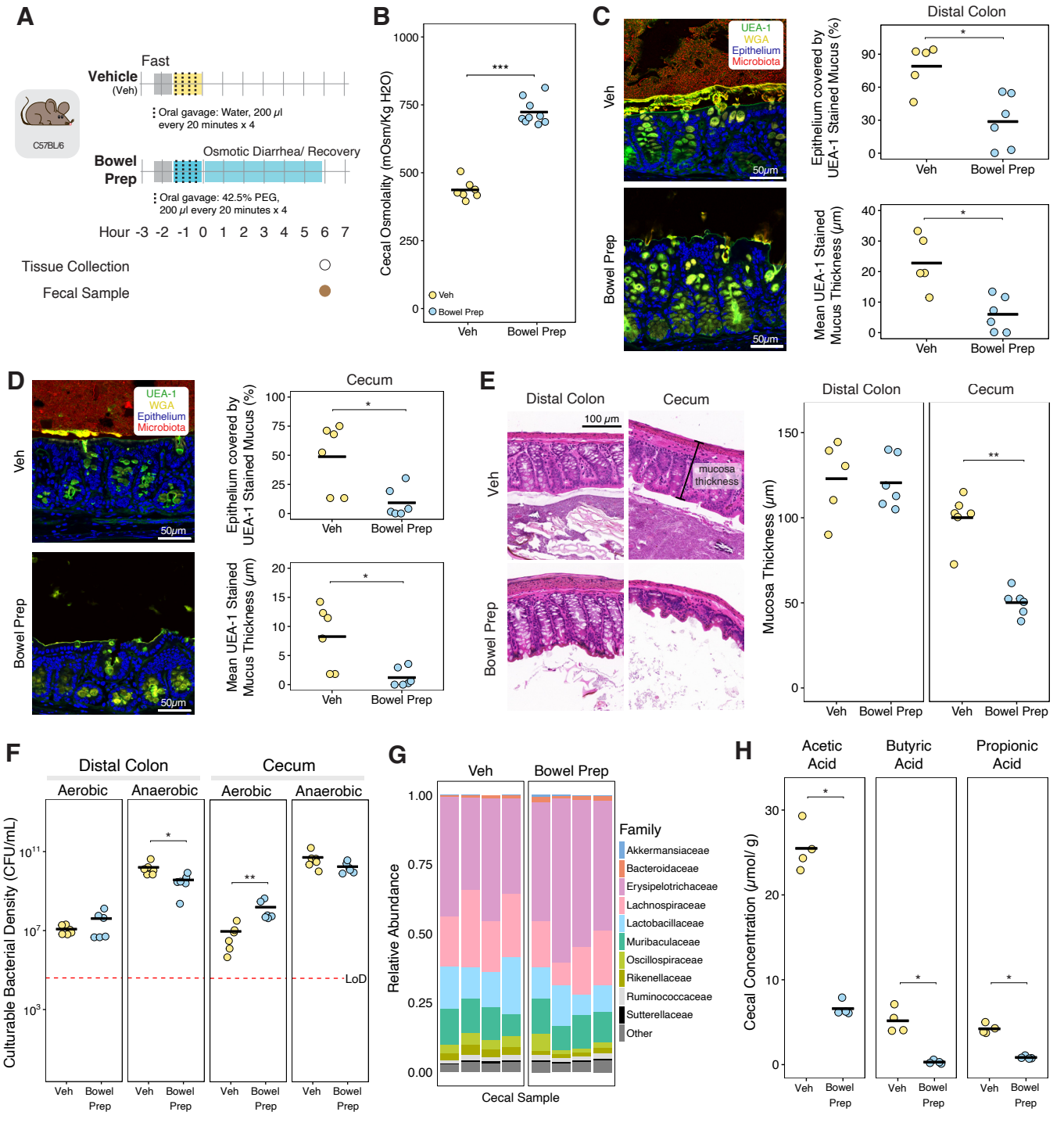
A
Fast
Vehicle
(Veh)
Oral gavage: Water, 200 μl
every 20 minutes x 4
C57BL/6
Osmotic Diarrhea/ Recovery
Bowel
Prep
Oral gavage: 42.5% PEG,
200 μl every 20 minutes x 4
Hour -3 -2 -1 0 1 2 3 4 5 6 7
Tissue Collection
Fecal Sample
B
Cecal Osmolality (mOsm/Kg H2O)
1000
750
500
250
0
***
Veh
Bowel Prep
C
UEA-1
WGA
Epithelium
Microbiota
Veh
Bowel Prep
50μm
Distal Colon
Epithelium covered by
UEA-1 Stained Mucus (%)
90
60
30
0
*
Mean UEA-1 Stained
Mucus Thickness (μm)
40
30
20
10
D
Cecum
Epithelium covered by
UEA-1 Stained Mucus (%)
100
75
50
25
Mean UEA-1 Stained
Mucus Thickness (μm)
20
15
10
5
E
Distal Colon
Cecum
100 μm
mucosa
thickness
Mucosa Thickness (μm)
150
100
50
0
**
F
Distal Colon
Cecum
Aerobic
Anaerobic
Culturable Bacterial Density (CFU/mL)
10^{11}
10^{7}
10^{3}
LoD
Veh
Bowel
Prep
G
Relative Abundance
1.00
0.75
0.50
0.25
0.00
Cecal Sample
Family
Akkermansiaceae
Bacteroidaceae
Erysipelotrichaceae
Lachnospiraceae
Lactobacillaceae
Muribaculaceae
Oscillospiraceae
Rikenellaceae
Ruminococcaceae
Sutterellaceae
Other
H
Acetic
Acid
Butyric
Acid
Propionic
Acid
Cecal Concentration (μmol/ g)
30
20
10
0

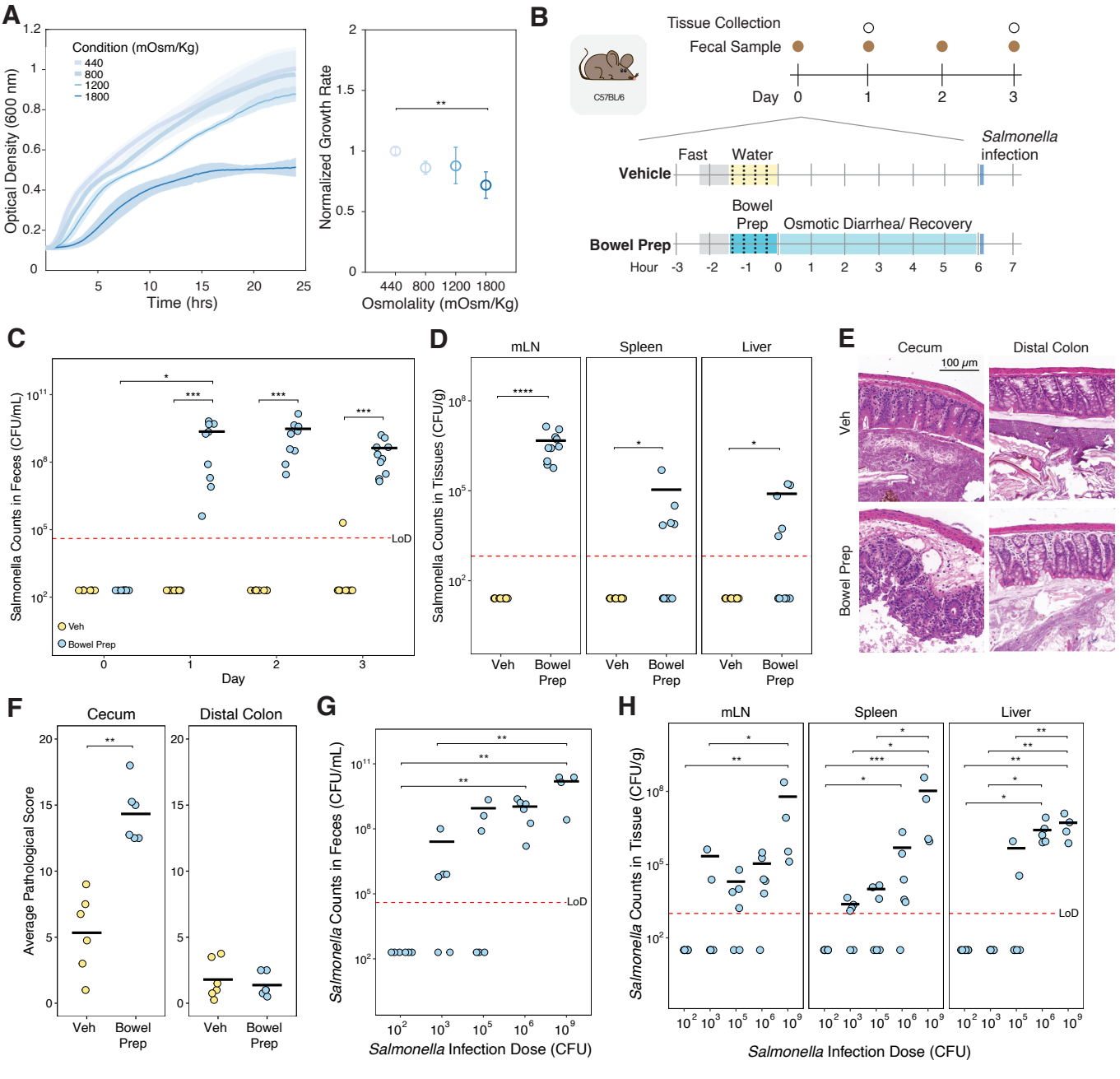
A
Condition (mOsm/Kg)
440
800
1200
1800
Optical Density (600 nm)
Time (hrs)
Normalized Growth Rate
Osmolality (mOsm/Kg)
B
Tissue Collection
Fecal Sample
Day
C57BL6
Fast
Water
Vehicle
Salmonella infection
Bowel Prep
Osmotic Diarrhea/ Recovery
Hour
C
Salmonella Counts in Feces (CFU/mL)
LoD
Veh
Bowel Prep
Day
D
mLN
Spleen
Liver
Salmonella Counts in Tissues (CFU/g)
Veh
Bowel Prep
E
Cecum
Distal Colon
100 μm
Veh
Bowel Prep
F
Cecum
Distal Colon
Average Pathological Score
Veh
Bowel Prep
G
Salmonella Counts in Feces (CFU/mL)
LoD
Salmonella Infection Dose (CFU)
H
mLN
Spleen
Liver
Salmonella Counts in Tissue (CFU/g)
LoD
Salmonella Infection Dose (CFU)

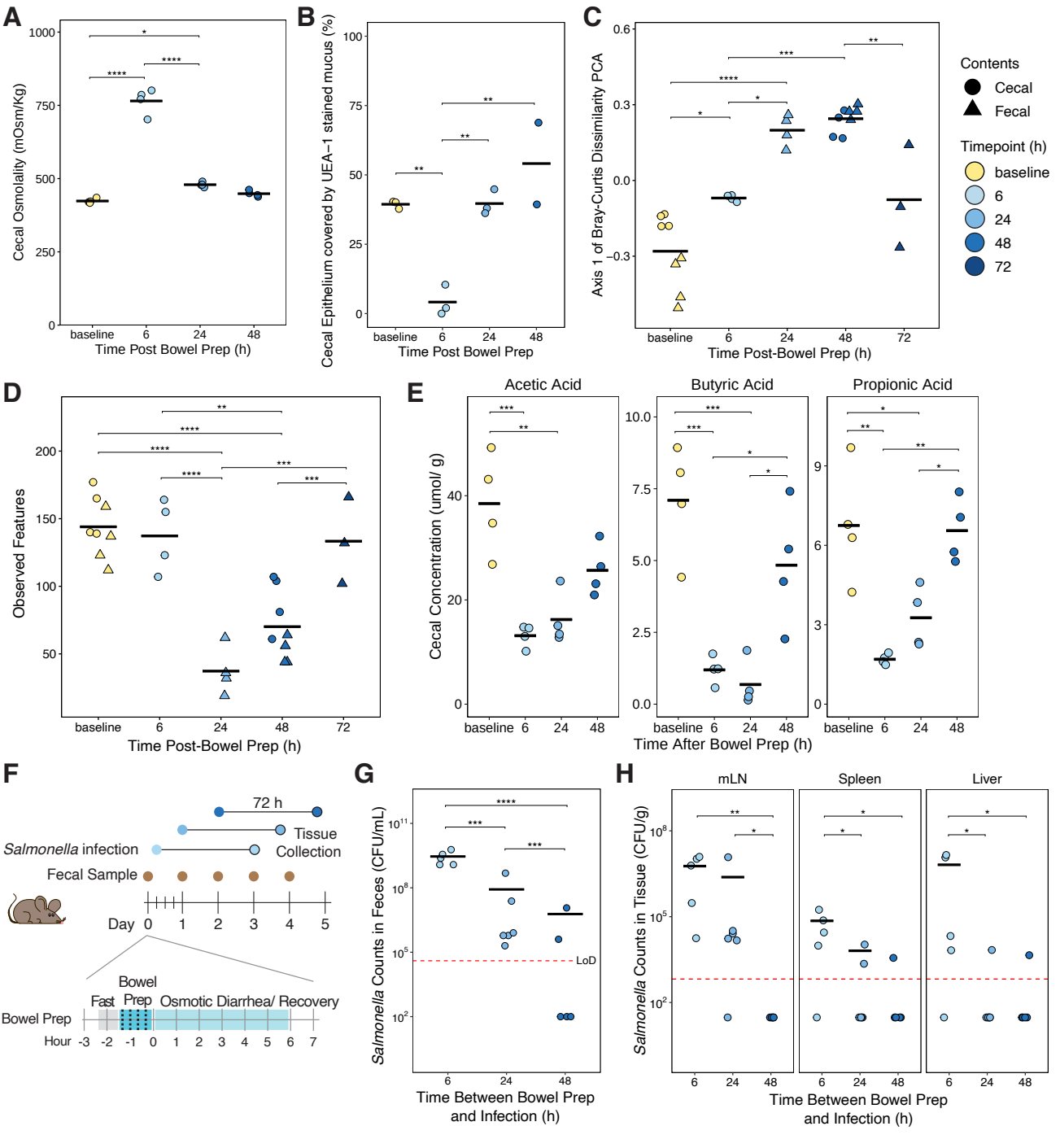
A
Cecal Osmolality (mOsm/Kg)
Time Post Bowel Prep (h)
baseline
6
24
48
B
Cecal Epithelium covered by UEA-1 stained mucus (%)
Time Post Bowel Prep
C
Axis 1 of Bray-Curtis Dissimilarity PCA
Time Post-Bowel Prep (h)
72
Contents
Cecal
Fecal
Timepoint (h)
baseline
6
24
48
72
D
Observed Features
Time Post-Bowel Prep (h)
E
Acetic Acid
Butyric Acid
Propionic Acid
Cecal Concentration (umol/ g)
Time After Bowel Prep (h)
F
72 h
Tissue Collection
Salmonella infection
Fecal Sample
Day 0 1 2 3 4 5
Bowel Prep
Fast
Bowel Prep
Osmotic Diarrhea/ Recovery
Hour -3 -2 -1 0 1 2 3 4 5 6 7
G
Salmonella Counts in Feces (CFU/mL)
LoD
Time Between Bowel Prep and Infection (h)
H
mLN
Spleen
Liver
Salmonella Counts in Tissue (CFU/g)
Time Between Bowel Prep and Infection (h)

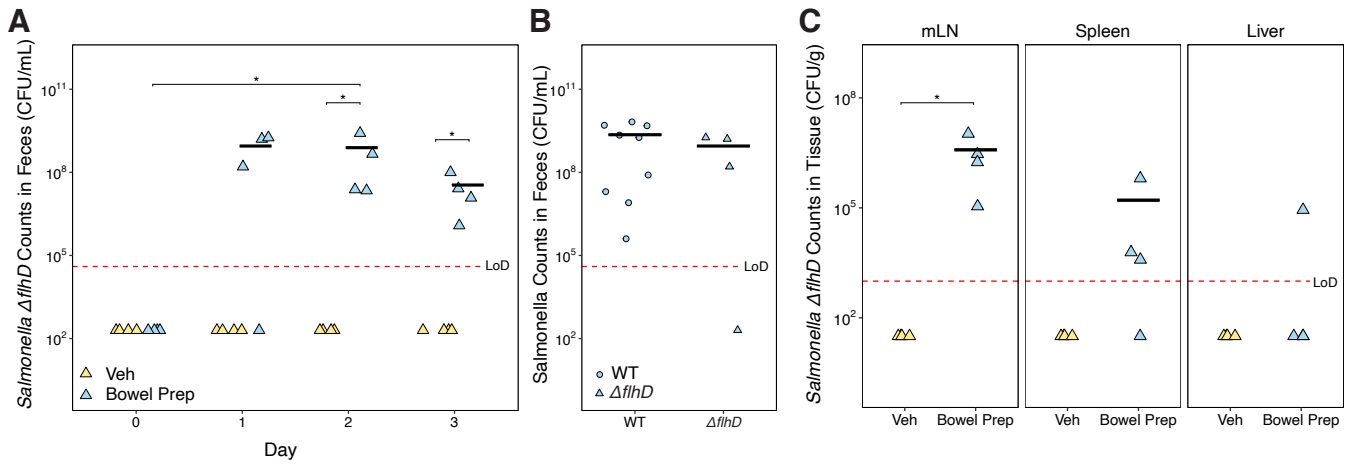
A
Salmonella ΔflhD Counts in Feces (CFU/mL)
10^11
10^8
10^5
10^2
LoD
*
*
*
Veh
Bowel Prep
0
1
2
3
Day
B
Salmonella Counts in Feces (CFU/mL)
10^11
10^8
10^5
10^2
LoD
WT
ΔflhD
WT
ΔflhD
C
mLN
Spleen
Liver
Salmonella ΔflhD Counts in Tissue (CFU/g)
10^8
10^5
10^2
LoD
*
Veh
Bowel Prep
Veh
Bowel Prep
Veh
Bowel Prep

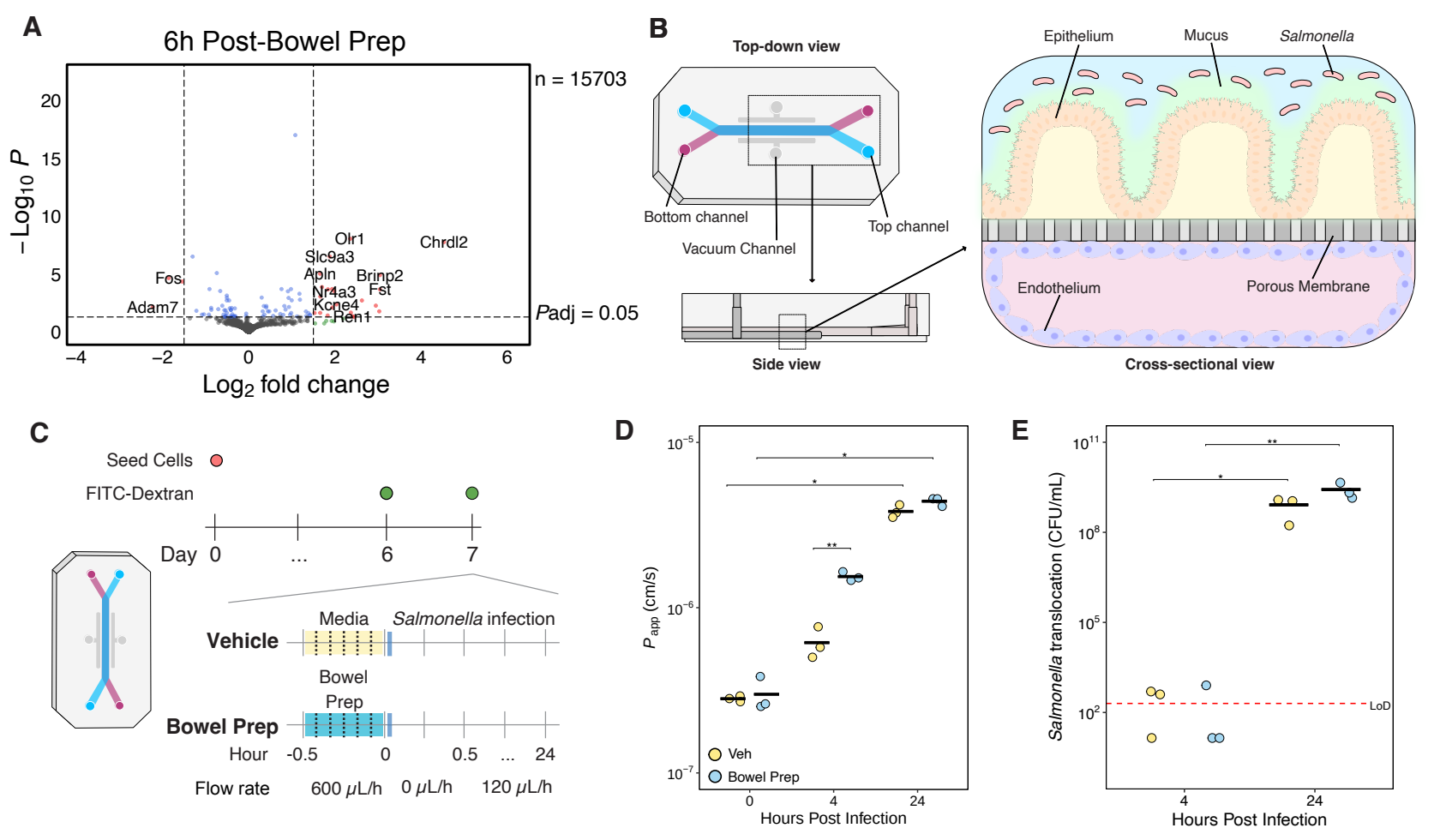
A
6h Post-Bowel Prep
n = 15703
Padj = 0.05
– Log10 P
Log2 fold change
Olr1
Chrdl2
Slc9a3
Apln
Brinp2
Fos
Nr4a3
Fst
Adam7
Kcne4
Ren1
B
Top-down view
Bottom channel
Vacuum Channel
Top channel
Side view
Epithelium
Mucus
Salmonella
Endothelium
Porous Membrane
Cross-sectional view
C
Seed Cells
FITC-Dextran
Day 0 ... 6 7
Media
Salmonella infection
Vehicle
Bowel Prep
Bowel Prep
Hour -0.5 0 0.5 ... 24
Flow rate 600 μL/h 0 μL/h 120 μL/h
D
Papp (cm/s)
Veh
Bowel Prep
Hours Post Infection
E
Salmonella translocation (CFU/mL)
LoD
Hours Post Infection

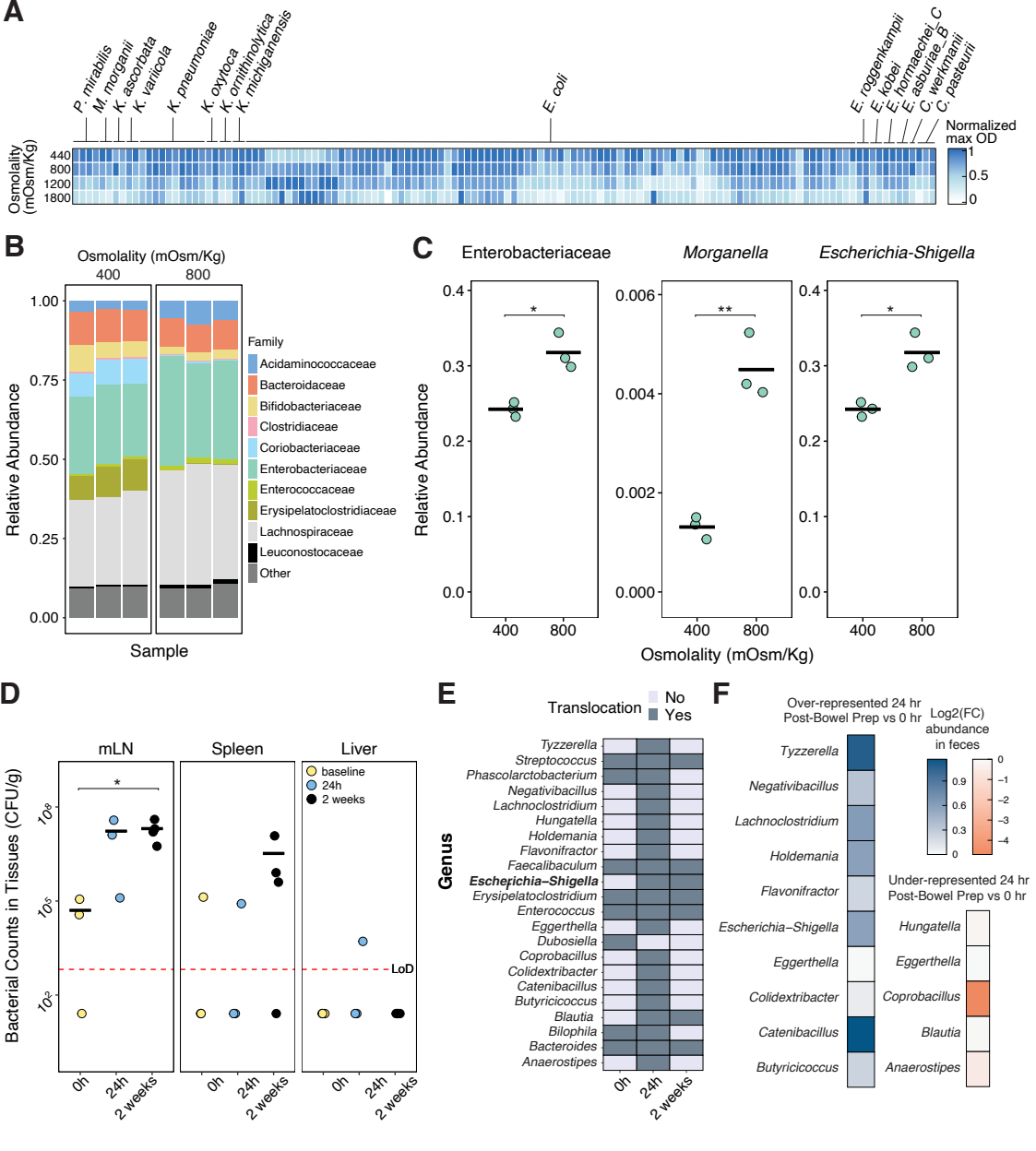
A
P. mirabilis
M. morganii
K. ascorbata
K. variicola
K. pneumoniae
K. oxytoca
K. ornithinolytica
K. michiganensis
E. coli
E. roggenkampii
E. kobei
E. hormaechei_C
E. asburiae_B
C. werkmanii
C. pasteurii
Normalized max OD
Osmolality (mOsm/Kg)
440
800
1200
1800
1
0.5
0
B
Osmolality (mOsm/Kg)
400
800
Relative Abundance
Sample
Family
Acidaminococcaceae
Bacteroidaceae
Bifidobacteriaceae
Clostridiaceae
Coriobacteriaceae
Enterobacteriaceae
Enterococcaceae
Erysipelatoclostridiaceae
Lachnospiraceae
Leuconostocaceae
Other
C
Enterobacteriaceae
Morganella
Escherichia-Shigella
Relative Abundance
Osmolality (mOsm/Kg)
D
mLN
Spleen
Liver
baseline
24h
2 weeks
Bacterial Counts in Tissues (CFU/g)
LoD
0h
24h
2 weeks
E
Translocation
No
Yes
Genus
Tyzzerella
Streptococcus
Phascolarctobacterium
Negativibacillus
Lachnoclostridium
Hungatella
Holdemania
Flavonifractor
Faecalibaculum
Escherichia–Shigella
Erysipelatoclostridium
Enterococcus
Eggerthella
Dubosiella
Coprobacillus
Colidextribacter
Catenibacillus
Butyricicoccus
Blautia
Bilophila
Bacteroides
Anaerostipes
F
Over-represented 24 hr Post-Bowel Prep vs 0 hr
Log2(FC) abundance in feces
Under-represented 24 hr Post-Bowel Prep vs 0 hr